NAVAL POSTGRADUATE SCHOOL

MONTEREY, CALIFORNIA

THESIS

PREDICTING THE EFFECTS OF SEA SURFACE SCATTER ON BROADBAND PULSE PROPAGATION WITH AN OCEAN ACOUSTIC PARABOLIC EQUATION MODEL

by

Richard M. Ead

June 2004

NPS Thesis Advisor:	Kevin B. Smith
NUWC Second Reader:	Daniel T. Nagle

Approved for Public Release; Distribution is Unlimited

THIS PAGE INTENTIONALLY LEFT BLANK

REPORT DOCUMENTATION PAGE			Form Approved OMB No. 0704-0188
Public reporting burden for this collection of information is estimated to average 1 hour per response, including the time for reviewing instruction, searching existing data sources, gathering and maintaining the data needed, and completing and reviewing the collection of information. Send comments regarding this burden estimate or any other aspect of this collection of information, including suggestions for reducing this burden, to Washington headquarters Services, Directorate for Information Operations and Reports, 1215 Jefferson Davis Highway, Suite 1204, Arlington, VA 22202-4302, and to the Office of Management and Budget, Paperwork Reduction Project (0704-0188) Washington DC 20503.			
1. AGENCY USE ONLY ***(Leave blank)***	**2. REPORT DATE** June 2004	**3. REPORT TYPE AND DATES COVERED** Master's Thesis	
4. TITLE AND SUBTITLE: Predicting the Effects of Sea Surface Scatter on Broad Band Pulse Propagation with an Ocean Acoustic Parabolic Equation Model			**5. FUNDING NUMBERS**
6. AUTHOR(S) Ead, Richard, M.			
7. PERFORMING ORGANIZATION NAME(S) AND ADDRESS(ES) Naval Postgraduate School Monterey, CA 93943-5000			**8. PERFORMING ORGANIZATION REPORT NUMBER**
9. SPONSORING /MONITORING AGENCY NAME(S) AND ADDRESS(ES) N/A			**10. SPONSORING/MONITORING AGENCY REPORT NUMBER**
11. SUPPLEMENTARY NOTES The views expressed in this thesis are those of the author and do not reflect the official policy or position of the Department of Defense or the U.S. Government.			
12a. DISTRIBUTION / AVAILABILITY STATEMENT Approved for public release; distribution is unlimited			**12b. DISTRIBUTION CODE**

13. ABSTRACT ***(maximum 200 words)***

Littoral waters when compared to the open ocean create an environment of greater reverberation with acoustic energy scattering from the sea surface, bottom, topographic features, and regions that lack homogeneity within the volume. If the ocean surface is rough on the scale of an acoustic wavelength, considerable scattering can occur that can significantly influence coherent propagation. Because the rough surface is also evolving dynamically, such scattering can introduce Doppler shifting and spreading of the acoustic pulse spectrum. This thesis builds upon prior efforts in ocean acoustic modeling and is focused on examining surface scattering and its affect upon coherent propagation. The dynamics/physics associated with surface scattering are explored in detail and mathematical relationships are developed and employed in revisions to the Monterey Miami Parabolic Equation (MMPE) model. The thesis provides background information associated with the MMPE and highlights earlier work related to surface scattering. It presents a formal analysis of an exact surface scattering approach in the context of a continuous wave (CW) benchmark exercise and the Doppler shifts associated with a dynamic rough surface. It expands on prior rough sea surface work to include modeling based on an empirical fetch-limited ocean wave spectrum and compares modeling results with measured data. Interest in broadband pulse propagation in shallow water is increasing with the need for improved active sonar systems and with the growth of applications such as underwater acoustic communications.

14. SUBJECT TERMS **Sea Surface Scatter, Parabolic Equation Model, Doppler Scatter, Bragg Scatter, JONSWAP Spectrum.**			**15. NUMBER OF PAGES** 93
			16. PRICE CODE
17. SECURITY CLASSIFICATION OF REPORT Unclassified	**18. SECURITY CLASSIFICATION OF THIS PAGE** Unclassified	**19. SECURITY CLASSIFICATION OF ABSTRACT** Unclassified	**20. LIMITATION OF ABSTRACT** UL

NSN 7540-01-280-5500 Standard Form 298 (Rev. 2-89)
Prescribed by ANSI Std. 239-18

THIS PAGE INTENTIONALLY LEFT BLANK

Approved for public release; distribution is unlimited

PREDICTING THE EFFECTS OF SEA SURFACE SCATTER ON BROADBAND PULSE PROPAGATION WITH AN OCEAN ACOUSTIC PARABOLIC EQUATION MODEL

Richard M. Ead
Naval Undersea Warfare Center Division Newport
B.S.E.E., University of Rhode Island, 1981

Submitted in partial fulfillment of the
requirements for the degree of

MASTER SCIENCE IN ENGINEERING ACOUSTICS

from the

NAVAL POSTGRADUATE SCHOOL
June 2004

Author: Richard M. Ead

Approved by: Kevin B. Smith
Thesis Advisor

Daniel T. Nagle
Second Reader

Kevin B. Smith
Chair, Engineering Acoustics Academic Committee

THIS PAGE INTENTIONALLY LEFT BLANK

ABSTRACT

Littoral waters when compared to the open ocean create an environment of greater reverberation with acoustic energy scattering from the sea surface, bottom, topographic features, and regions that lack homogeneity within the volume. If the ocean surface is rough on the scale of an acoustic wavelength, considerable scattering can occur that can significantly influence coherent propagation. Because the rough surface is also evolving dynamically, such scattering can introduce Doppler shifting and spreading of the acoustic pulse spectrum. This thesis builds upon prior efforts in ocean acoustic modeling and is focused on examining surface scattering and its affect upon coherent propagation. The dynamics/physics associated with sea surface scattering are explored in detail and mathematical relationships are developed and employed in revisions to the Monterey Miami Parabolic Equation (MMPE) model. The thesis provides background information associated with the MMPE and highlights earlier work related to surface scattering. It presents a formal analysis of an exact surface scattering approach in the context of a continuous wave (CW) benchmark exercise and the Doppler shifts associated with a dynamic rough surface. It expands on prior rough sea surface work to include modeling based on an empirical fetch-limited ocean wave spectrum and compares modeling results with measured data. Interest in broadband pulse propagation in shallow water is increasing with the need for improved active sonar systems and with the growth of applications such as underwater acoustic communications.

THIS PAGE INTENTIONALLY LEFT BLANK

TABLE OF CONTENTS

THIS PAGE INTENTIONALLY LEFT BLANK

LIST OF FIGURES

LIST OF ACRONYMS

BELLHOP	Gaussian beam tracing model
CW	Continuous Wave
FFT	Fast Fourier Transform
JONSWAP	Joint North Sea Wave Observation Project
MMPE	Monterey Miami Parabolic Equation Model
PE	Parabolic Equation
SSF	Split Step Fourier
UMPE	University of Miami Parabolic Equation Model
WAPE	Wide Angle Parabolic Equation

THIS PAGE INTENTIONALLY LEFT BLANK

ACKNOWLEDGMENTS

This thesis represents the culmination of the author's efforts toward a Master of Science Degree in Engineering Acoustics and is the result of participating in a distance learning program established in 2000 between the Naval Postgraduate School and the Naval Undersea Warfare Center Division Newport.

The author would like to express his appreciation to Dr. Daniel T. Nagle for his time reading the work and providing helpful comments and to Dr. Mohsen Badiey for his help with the HFA97 experiment data. Furthermore, the author extends his sincerest gratitude to Prof. Kevin Smith for his guidance and expertise during the development of this thesis.

The author would also like to thank his dear wife, Margaret, for her patience and encouragement which were so important to the success of this work.

THIS PAGE INTENTIONALLY LEFT BLANK

I. INTRODUCTION

A. THESIS OBJECTIVES AND MOTIVATION

The principal objectives of this thesis are to demonstrate the capability to model the complex physical interactions associated with acoustic broadband pulse propagation reflecting from a rough sea surface. The sea surfaces modeled include cases for static and dynamic simple surfaces and more complicated realizations of static surfaces.

Littoral waters when compared to the open ocean create an environment of greater reverberation with acoustic energy scattering from the sea surface, bottom, topographic features, and regions lacking homogeneity within the volume. If the ocean surface is rough on the scale of an acoustic wavelength, considerable scattering can occur that can significantly influence coherent propagation. Because the rough surface is also evolving dynamically, such scattering can introduce Doppler shifting and spreading of the acoustic pulse spectrum. Interest in broadband pulse propagation in shallow water is increasing with the need for improved active sonar systems and with the growth of applications such as underwater acoustic communications. Also, determining sea surface roughness presents an inverse problem of interest in which acoustic waves can possibly be used as a tool to understand the physical environment.

B. SUMMARY

This thesis builds upon prior efforts in ocean acoustics modeling and is focused on examining surface roughness and its affect upon coherent propagation. The dynamics/physics associated with ocean sea surface roughness are explored in detail and mathematical relationships are developed and employed in revisions to the Monterey Miami Parabolic Equation (MMPE) model.

Section II covers background information in detail associated with the MMPE and highlights earlier work related to surface scattering. Much of this earlier work centers on the use and upgrade of acoustic propagation codes based on the split-step Fourier parabolic equation algorithm introduced by Hardin and Tappert (1973). As an upgrade, Tappert and Nghiem-Phu (1985) developed an algorithm to compute exact surface forward scatter when the surface interface is not assumed to be flat. An approximate rough surface scatter was later developed and published in a University of Miami Parabolic Equation (UMPE) technical report (Smith and Tappert, 1993). Other published references to the approximate scatter approach are found in two theses (Wei Li, 1993, and Jun He, 1997).

Section II also describes implementation of the MMPE model and details such as operation of the model can be found on the Ocean Acoustics Library website at http;//oalib.saic.com/PE/index.html. Section II concludes with a literature search of earlier work showing how surface waves act as moving diffraction gratings, scattering low frequency sound in selected, well defined directions and imparting a unique Doppler shift in each direction.

Sections III and IV cover a formal analysis of an exact surface scattering approach in the context of a continuous wave (CW) benchmark exercise and the Doppler shifts associated with a dynamic rough surface. Section III implements into the MMPE model a static rough surface forward scatter subroutine similar in function to what has been developed for the UMPE model. The influence of a simple sinusoidal surface perturbation is examined and Doppler effects from a dynamic ocean surface are computed. Section IV sets up the model to calculate Doppler shifts in the presence of a dynamically moving surface and verifies that the updated model performs adequately. A benchmark exercise is conducted with the results showing the expected frequency spectra at different depths and different ranges.

Section V expands on the rough sea surface work to include modeling based on an empirical fetch-limited ocean wave spectrum and compares modeling results with

measured data. The Pierson-Moskowitz spectrum is presented showing energy spectra for fully developed waves at various wind speeds. Next, an experiment conducted in 1997 (HFA97) measuring cause and effect between the ocean environment and acoustic propagation is analyzed. The MMPE model is updated with the JONSWAP wave spectrum with results clearly showing surface reflected paths dispersing acoustic energy at increasing rates as wind speed increases, and also clearly showing how the direct path (non-surface interaction) remains unchanged. MMPE Model statistics are computed for standard deviation of arrival angle and arrival time and compared with both HFA97 measured data, and data from another model (BELLHOP/JONSWAP).

Conclusions and recommendations are discussed in Section VI. The results presented show that surface scatter can significantly affect arrival time, arrival angle, and frequency spread that leads to degradation of acoustic signal coherence. Some recommendations for future work include examining Doppler shifts for the dynamically evolving rough surface case, improving upon data processing MATLAB Algorithms, and validating algorithms with additional measured data.

THIS PAGE INTENTIONALLY LEFT BLANK

II. PREVIOUS WORK

A. BACKGROUND AND DESCRIPTION OF MMPE MODEL

1. Analytical Development of MMPE

Hardin and Tappert (1973) are two of the earlier contributors to have applied a parabolic approximation of the acoustic wave equation to predict underwater sound propagation. Since then, parabolic equation models have become the models of choice in cases where the environment varies with range.

The predecessor to the Monterey Miami Parabolic Equation (MMPE) model (Smith, 2001) is the University of Miami Parabolic Equation (UMPE) model developed as a research model under the guidance of Professor Fred Tappert (Smith and Tappert, 1993). The MMPE is based on most of the same approximations and numerical algorithms as the previous UMPE model with a few exceptions. The most notable change includes the centered-step scheme of the split-step Fourier algorithm. This change improves accuracy in the range-step calculation by an order of magnitude while adding a fractional amount to the overall run time.

The MMPE model is derived by beginning with the definition of the Helmholtz wave equation in cylindrical coordinates,

$$\nabla^2 p(r,z) + K_o^2 n^2(r,z)\ p(r,z) = 0\ . \qquad (2.1)$$

Equation (2.1) is then factored by introducing the operator notation

$$Q_{op} = (\mu + \varepsilon + 1)^{\frac{1}{2}} \quad , \qquad (2.2)$$

where

$$\mu = \frac{1}{k_o^2}\frac{\partial}{\partial z^2} \ , \tag{2.3}$$

$$\varepsilon = n^2 - 1 \ , \tag{2.4}$$

and

$$n = \frac{c_o}{c} \ . \tag{2.5}$$

The outgoing pressure field may then be defined in terms of the parabolic equation (PE) field function, ψ, according to the following equation,

$$p(r,z) = P_o \sqrt{\frac{R_o}{r}} \ Q_{op}^{-1/2} \, \psi(r,z) \, e^{ik_o r} \quad , \tag{2.6}$$

where ψ satisfies a parabolic equation of the type

$$\frac{\partial \psi}{\partial r} = -ik_o \psi + ik_o Q_{op} \psi = -ik_o H_{op} \psi \quad . \tag{2.7}$$

The split-step Fourier algorithm (Hardin and Tappert, 1973) is then applied by separating the "Hamiltonian" operator, H_{op}, into the sum of "kinetic energy" and "potential energy" operators, T_{op} and U_{op}, such that the field is marched outward in range according to

$$\psi(r+\Delta r, z) = e^{-ik_o \frac{\Delta r}{2} U_{op}(r+\Delta r, z)} \ FFT\left\{ e^{-ik_o \Delta r \, \hat{T}(k_z)} \ IFFT\left(e^{-ik_o \frac{\Delta r}{2} U_{op}(r,z)} \ \psi(r,z) \right) \right\} \ . \tag{2.8}$$

In the MMPE model, the expressions for the operator approximations employ the wide angle PE (WAPE) forms (Thompson and Chapman, 1983),

$$U_{op}(r,z) = -\left[n(r,z)-1\right] \quad \text{and} \quad \hat{T}_{op}(k_z) = 1-\left[1-\left(\frac{k_z}{k_o}\right)^2\right]^{1/2}. \qquad (2.9)$$

Finally, in terms of the surface reflection, the pressure release boundary condition is imposed at each range step by forcing the odd symmetry constraint

$$\psi(-z) = -\psi(z)\ , \qquad (2.10)$$

which requires the use of an "image ocean" solution when using the full FFT form (rather than a simpler sine transform for z>0). Further details of the MMPE implementation can be found in the review article by Smith (2001).

In the case of a rough surface, the pressure release boundary condition must still be satisfied, but now it is imposed at the position of the displaced surface defined by

$$z-\eta(r) = 0\ , \qquad (2.11)$$

such that

$$\psi(z=\eta(r) = 0\,. \qquad (2.12)$$

Tappert and Nghiem-Phu (1985) showed that this can be achieved by defining the U_{op} operator (dependent on the environmental index of refraction) as an even function and the field function ψ as an odd function about the displaced surface interface, and then solving two parabolic equations, one for the real ocean and one for the image, defined by

real ocean: $$\frac{\partial\psi}{\partial r} = -ik_0\left(T_{op}+U_{op}\right)\psi, \qquad z > \eta(r), \qquad (2.13)$$

and

image ocean: $$\frac{\partial \psi}{\partial r} + 2\frac{\partial \eta}{\partial r}\frac{\partial \psi}{\partial z} = -ik_0\left(T_{op} + U_{op}\right)\psi, \qquad z > \eta(r). \tag{2.14}$$

It can be shown that

$$\psi\left(r, -z + 2\eta(r)\right) = -\psi(r, z), \tag{2.15}$$

or

$$\psi\left(r, \eta(r)\right) = 0, \tag{2.16}$$

as required.

The two parabolic equations are transformed into the single form previously defined by introducing a new field function extending over both real and image ocean depths defined by

$$\tilde{\psi}(r, z) = \begin{cases} \psi(r, z), & z > \eta(r) \\ -e^{i2k_0\frac{\partial \eta}{\partial r}(z-n)}\,\psi\left(r, -z + 2\eta(r)\right), & z < \eta(r) \end{cases}. \tag{2.17}$$

This new field function then satisfies the previous parabolic equation form at all depths, but with an altered U_{op}, i.e.

$$\frac{\partial \tilde{\psi}}{\partial r} = -ik_0\left(T_{op} + \tilde{U}_{op}\right)\tilde{\psi}\ , \tag{2.18}$$

where

$$\tilde{U}_{op}(r, z) = \begin{cases} U_{op}(r, z), & z > \eta(r) \\ U_{op}(r, z) - 2(z - \eta)\frac{\partial^2 \eta}{\partial r^2}, & z < \eta(r) \end{cases}. \tag{2.19}$$

2. Implementation of MMPE

The code for the MMPE was developed in Fortran and is accessible with a Fortran compiler such as Digital Visual Fortran Development Studio. Details as to the makeup and operation of the model can be found on the Ocean Acoustics Library website at http;//oalib.saic.com/PE/indel.html.

The model's executable file, mmpe2dbb.exe, is compiled from six source files and calls seven ascii input files during operation. These files contain information on run parameters, source parameters, and all necessary environmental information.

When the program is run, a single output binary file is created in which is contained a header and the vast majority of the remaining file is the PE field function $\psi(r, z)$. The mmpe2dbb executable is a broadband version of the 2-D PE model.

Two post-processing files developed in MATLAB code process the binary file data. To initialize the output processing one program (peout1) is run (in MATLAB) which reads the header and provides file identification for further analysis. Next, a second program (peout2) is run (in MATLAB) which provides menus for selecting various options for processing the data. Figure 2.1 shows the MATLAB display results of computing data for a single radial with a source frequency of 400 Hz, a source depth of 50 meters, a water depth of 250 meters, and at a range of 10 km for a simple, range-independent environment.

B. LITERATURE SEARCH

Warfield (1981) describes Doppler shift scattered from the ocean surface well in his article titled "Doppler Shifting of Surface-Scattered Reverberation". The underlying physical mechanism is that gravity waves on the ocean surface act as moving diffraction gratings, scattering low-frequency sound in selected, well-defined directions and

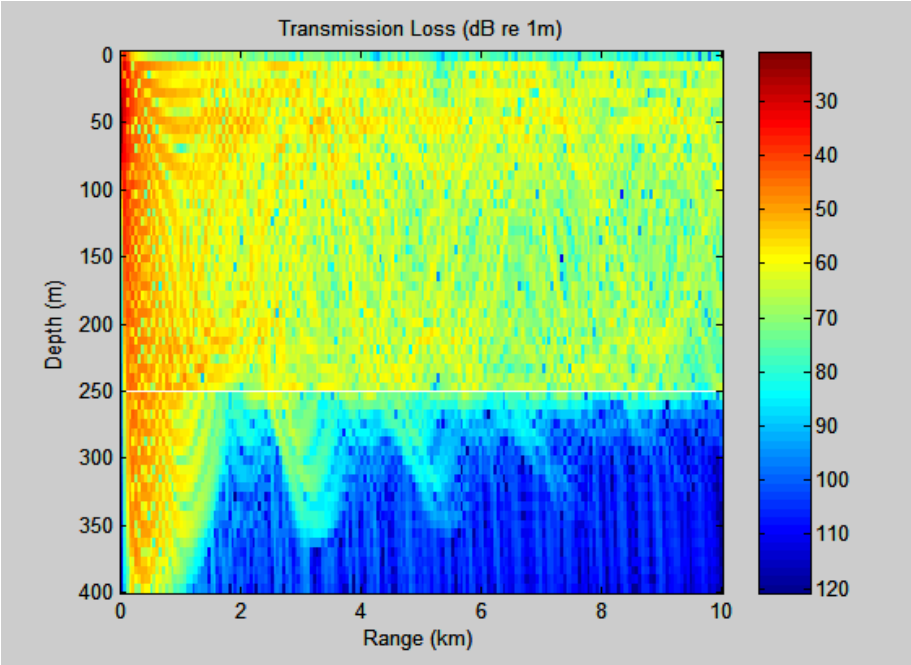

Figure 2.1 Transmission Loss vs. Depth and Range

imparting a unique Doppler shift in each direction. One aspect of the reverberation problem that appears to be well in hand is the Doppler shift of CW plane waves scattered from the ocean surface and sensed by a directional receiver.

Liebermann (1963) showed that backscatter of sound waves in air from a moving water surface preferentially selects a wavelength from the water surface spectrum according to the familiar diffraction-grating equation. Since each wavelength has a characteristic speed, the backscatter has a characteristic Doppler shift (even though no basic wave physics analysis was presented to indicate why the diffraction-grating equation should work); his experiment was probably the breakthrough result on the problem.

Marsh (1963) presented an analysis shortly after Liebermann of the Doppler shift of boundary reverberation based on scattering theory. His analysis gave an expression for bistatic reverberation spectra in which the Doppler shift is determined according to a diffraction-grating relationship.

III. UPDATED MMPE FOR SURFACE SCATTERING

A. STATIC ROUGH SURFACE MODELING

The first modification to the MMPE code was to provide a representation of a static rough surface. A rough surface forward scatter subroutine (ZSGEN) similar in function to what has been developed for the UMPE model was added to the MMPE to calculate a roughness spectrum. For the purpose of computing the acoustic field in two dimensions (depth and range), only a 1-D roughness spectrum along the track of interest was needed.

The subroutine ENVPROP was modified to perform a calculation of an image ocean potential function. The output data from ZSGEN provides the input for this calculation. Again, the modifications are similar to what has been implemented previously in the UMPE. The surface is treated as a perfect reflector due to a pressure release boundary. With this method, we assume an identical image ocean overlays the real ocean for negative values of depth and, furthermore, the acoustic field is exactly equal but of opposite sign in the image ocean.

The main routine, PEMP, was updated to compute exact rough surface scatter and transform the results to the physical space domain. When the model is run, the user is able to explicitly define the rms surface roughness (see Fig. 3.1).

The model was run with an rms roughness of 1, 5, and 10 meters. The input parameters are as follows: source depth of 50 m, center frequency of 400 Hz, maximum range of 10 km, maximum depth of 400 m, and single radial output.

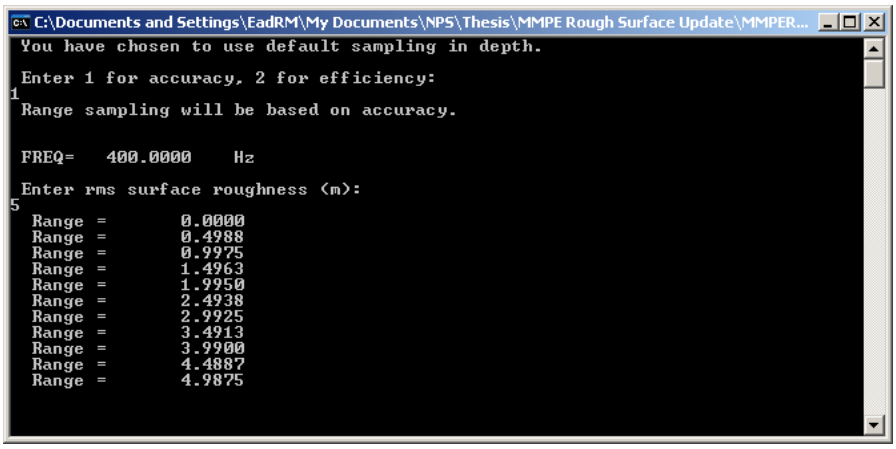

Figure 3.1 Model Running Display

Figures 3.2, 3.3, and 3.4 show results for an rms roughness of 1, 5, and 10 m respectively. Note the increase in near surface attenuation as the rms roughness increases.

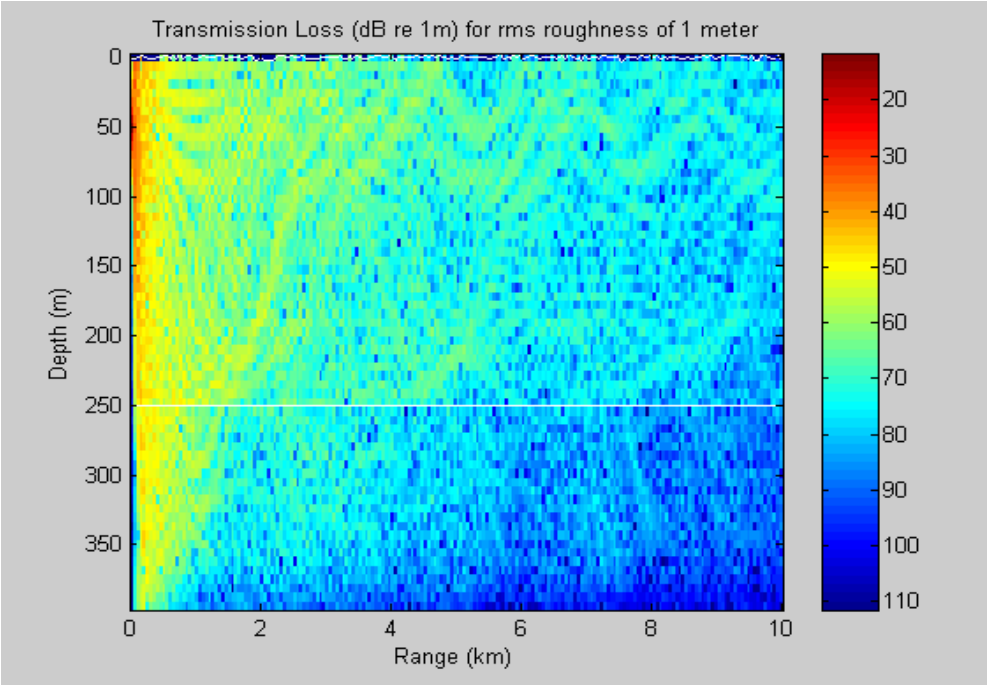

Figure 3.2 Transmission Loss for rms Roughness of 1 m at 400 Hz

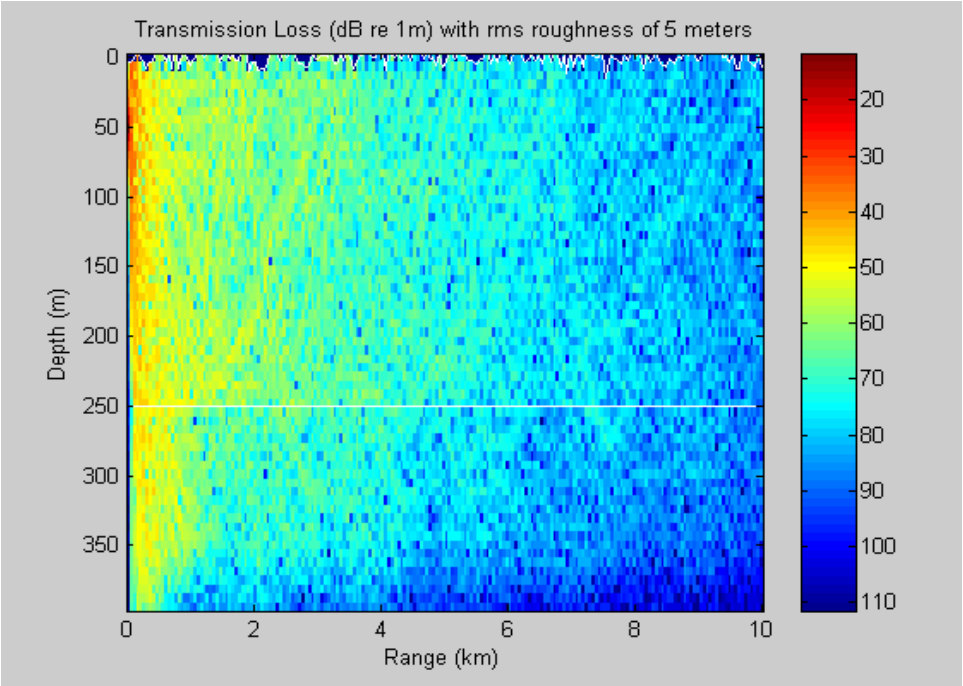

Figure 3.3 Transmission Loss for rms Roughness of 5 m at 400 Hz

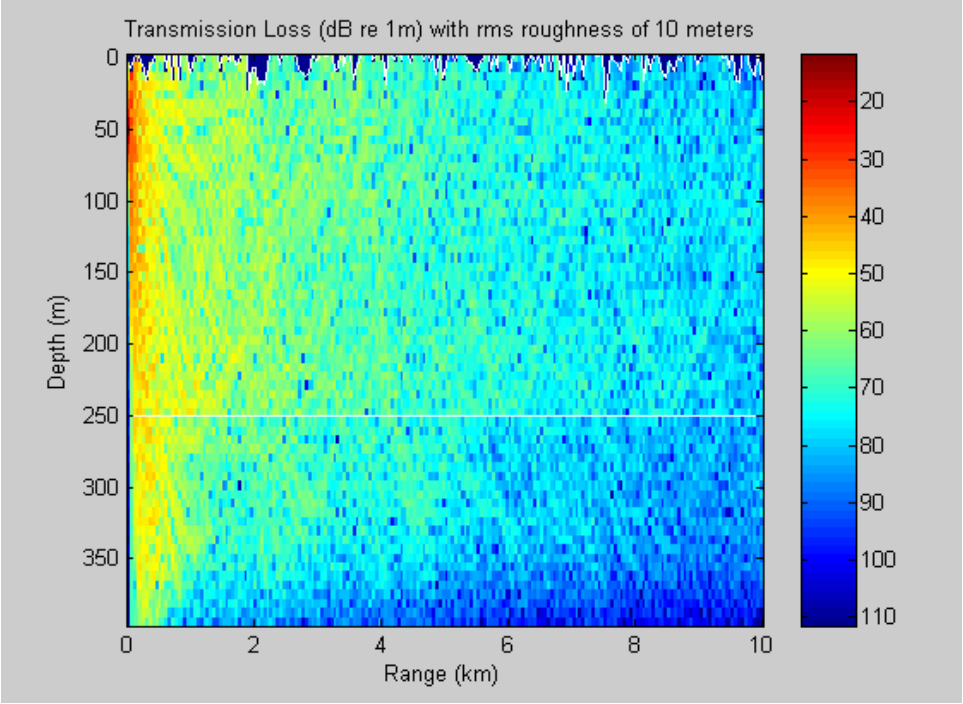

Figure 3.4 Transmission Loss for rms Roughness of 10 m at 400 Hz

B. SCATTERING FROM A SIMPLE SINUSOIDAL SURFACE

As a test of the exact forward scatter model, and to introduce the ability to compute Doppler effects from a dynamic ocean surface, we examine the influence of a simple sinusoidal surface perturbation. A sinusoidal perturbation will create Bragg resonant (diffraction grating) scattering, where the reflected field will be concentrated around the Bragg lines (see Fig 3.5) which satisfy the following:

$$\cos\theta_{r,n} = \cos\theta_i \pm n\frac{\lambda}{\lambda_w}, \tag{3.1}$$

where $\lambda \equiv$ acoustic wavelength, $\lambda_w \equiv$ surface wave wavelength, $\theta_i \equiv$ incident angle, and $\theta_{r,n} \equiv$ reflected angles.

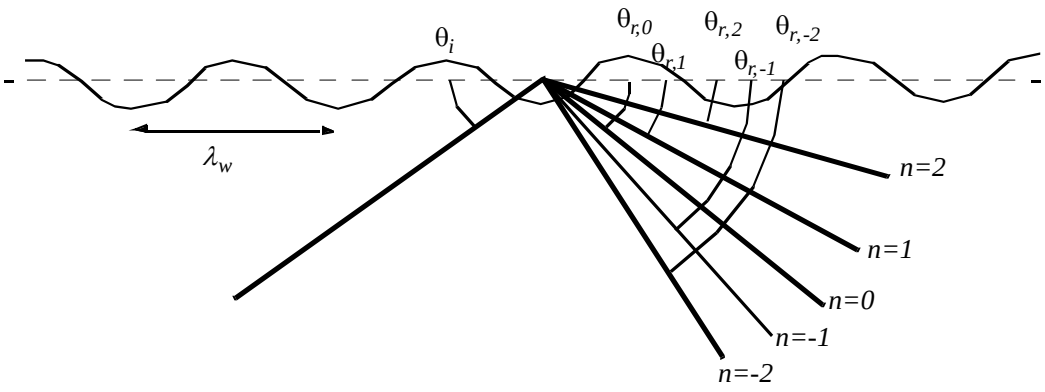

Figure 3.5 Depiction of Bragg scatter

For the test case conducted, we set $f = 1500$ Hz, c=1500 m/s, $\lambda = 1$ m, and $\lambda_w = 20$ m.

Then

$$\frac{\lambda}{\lambda_w} = \frac{1}{20} = 0.5 \tag{3.2}$$

If $\theta_i = 30^{\mathrm{O}}$, the Bragg lines occur at

$$\theta_{r,0} = 30^{\mathrm{O}}$$

$$\theta_{r,1} = 23.6^{\mathrm{O}} \qquad \theta_{r,-1} = 35.3^{\mathrm{O}}$$

$$\theta_{r,2} = 15.0^{\mathrm{O}} \qquad \theta_{r,-2} = 40.0^{\mathrm{O}}$$

$$\theta_{r,3} = \textit{complex} \qquad \theta_{r,-3} = 44.3^{\mathrm{O}}$$

It was determined empirically that the updated MMPE needs good depth resolution of the surface displacement (Z). For a maximum displacement of Z, the depth mesh should sample at least by Z/5 (or better). For small surface roughness this puts a large computational burden on the model because it requires very fine depth increments. Further, it hasn't been determined what minimum value of roughness can be ignored (though it should be dependent on the acoustic wavelength). Also, the model was written in such a way that the surface displacement is simply rounded to the nearest depth mesh.

To observe Bragg scattering requires an incident plane wave from which the reflected/scattered energy is observed propagating in specific directions. This was accomplished by assuming the source was a long (1000 m) vertical array steered towards the surface (D/E of -30°).

The subroutine ENVPROP was modified to input from the operator the surface wave speed and the time of surface realization. Sinusoidal surface displacement was then calculated. The model was run first simulating a flat surface (0 m roughness). It was then run with 5m rms roughness. The MATLAB output subroutine PEOUT2 was also modified to display the upper part of the water column only (the better to observe Bragg scattering).

The sound speed profile file was set to isothermal conditions at 1500 m/s. The model was run with settings that limit the output of depth data to 400 meters in order to save on processing and storage time. The maximum range was limited to 4 km.

Figure 3.6 shows results from the interaction in the upper part of the water column of the plane wave reflecting from a flat (0 m roughness) surface. Figure 3.7 shows modeling results using a 5 m amplitude sine wave surface roughness with a surface wavelength of 20 meters. The absolute value of the difference between the complex pressures computed in each case is presented in Fig. 3.8. Figure 3.9 is a plot with the same data as Fig. 3.8 but now the Bragg lines have been superimposed on the figure at the proper Bragg angles.

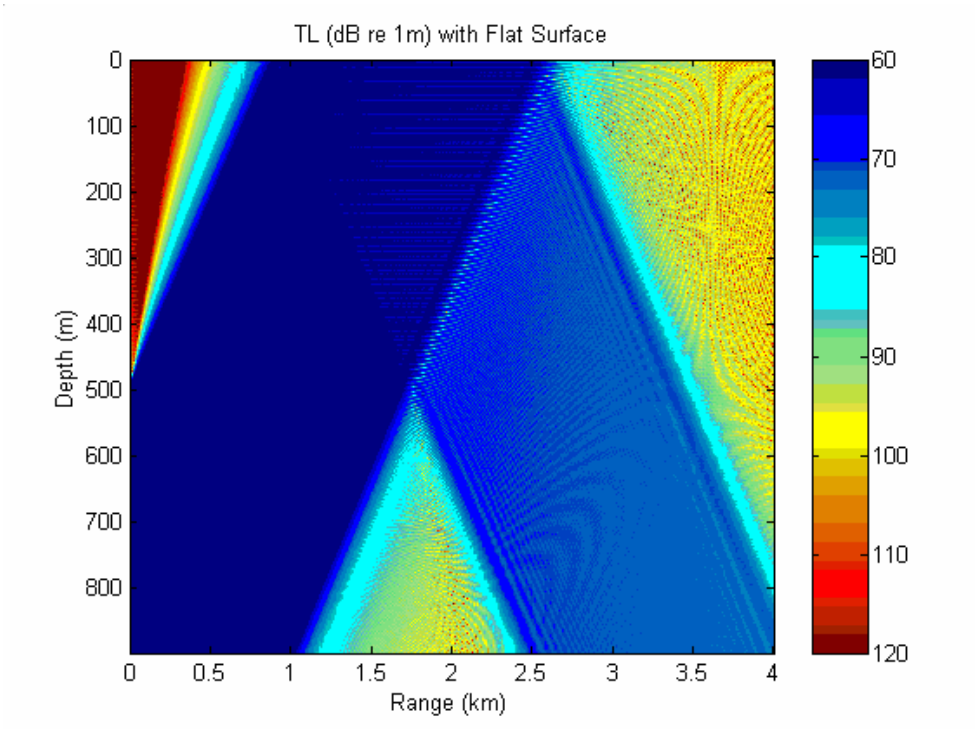

Figure 3.6 Flat Surface Interaction from Upper Part of Water Column

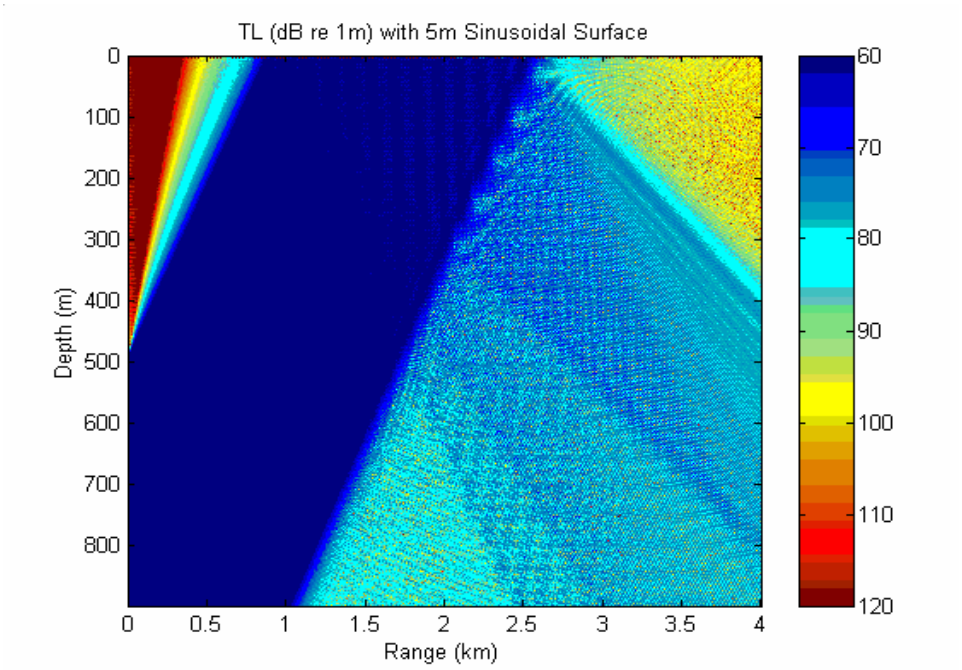

Figure 3.7 5m Roughness

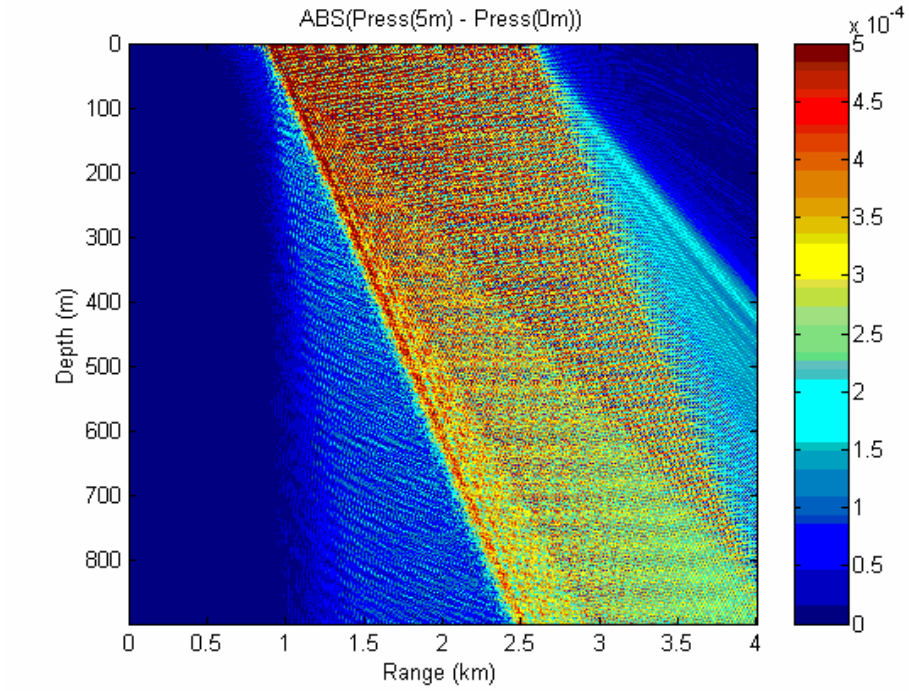

Figure 3.8 Absolute Value Difference

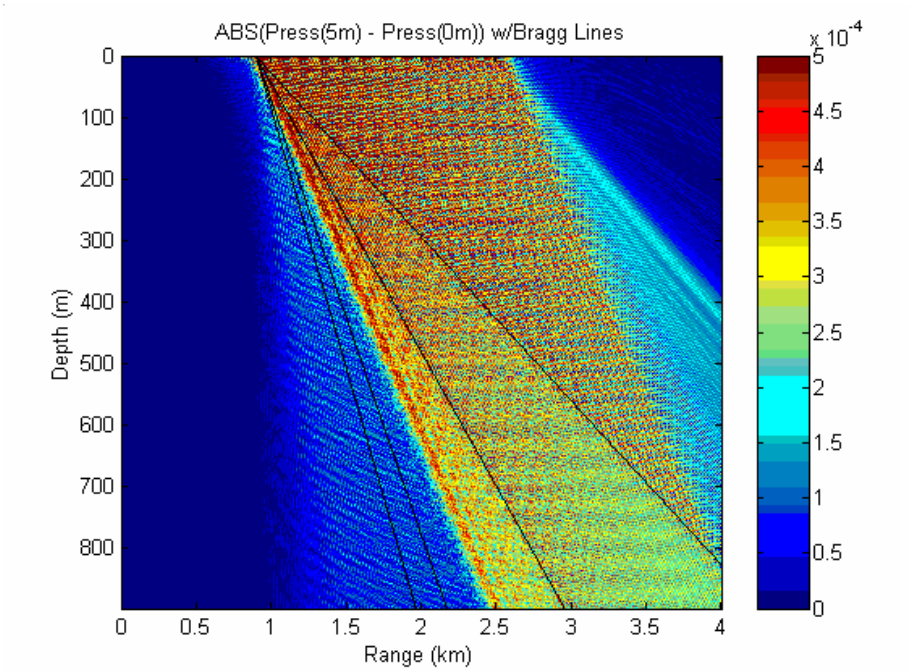

Figure 3.9 Bragg Lines Superimposed on Difference Plot

IV. SIMPLE TEST OF DYNAMIC SURFACE-INDUCED DOPPLER SPREAD

The focus in this section is setting up the model to calculate Doppler shifts in the presence of a dynamically moving surface and to verify that the updated model performs adequately.

A. INCORPORATING SIMPLE, DYNAMIC SINUSOIDAL SURFACE

For a moving surface wave with frequency ω_w, the surface wave number is

$$k_w = \frac{2\pi}{\lambda_w}, \tag{4.1}$$

and the surface displacement phase speed will be

$$v_w = \frac{\omega_w}{k_w} = \frac{\lambda_w \omega_w}{2\pi} \ . \tag{4.2}$$

The scattered beams will then undergo a Doppler shift according to (Medwin and Clay, 1998)

$$\omega_r = \omega_i \left[1 + \frac{v_w}{c} \left(\cos\theta_r - \cos\theta_i \right) \right]$$

$$= \omega_i \left[1 \pm \frac{v_w}{c} n \frac{\lambda}{\lambda_w} \right]$$

$$= \omega_i \left[1 \pm \frac{n\lambda}{c} \frac{\omega_w}{2\pi} \right], \tag{4.3}$$

or with $f = \frac{\omega}{2\pi}$,

$$f_r = f_i \left[1 \pm n \frac{f_w}{f_i} \right] = f_i \pm n f_w \ , \tag{4.4}$$

so

$$f_w = \frac{\omega_w}{2\pi} = \frac{v_w k_w}{2\pi} = \frac{v_w}{\lambda_w} \ . \tag{4.5}$$

Recall the following for the test case in Chapter III: f=1500 Hz, c=1500 m/s, $\lambda = 1\,\text{m}$, and $\lambda_w = 20\,\text{m}$. To make this noticeable at $f_i = 1500\,\text{Hz}$, we desire $f_w \approx 50$ Hz. This requires that $v_w = \lambda_w f_w = 1000$ m/s! This is not realistic, but will be used to test the model.

To ensure adequate sampling of a 20 m wavelength moving surface wave, we should sample roughly every 2 – 4 m. Since the surface wave is moving at 1000 m/s, this suggests a minimum sampling rate of $f_s = 250\,\text{Hz}$. Furthermore, since the Doppler is $\approx 50\,\text{Hz}$, we should sample in frequency at least every 5-10 Hz, thereby requiring a time sample length of at least $T = 0.256\,\text{sec}$.

Based on these requirements, the model was run 128 times with time steps of $\Delta t = 2$ msec ($f_s = 500\,\text{Hz}$) for a maximum time span of $T = 0.256\,\text{sec}$. At each time sample, the surface displacement was computed from

$$\eta(r) = A \sin\left[\frac{2\pi}{\lambda_w} (r + v_w t) \right], \tag{4.6}$$

where A is the surface wave amplitude, set to 5 m. The resulting 128 point time series data were extracted at various positions within the field and Fourier transformed to observe Doppler shifts.

Next, data was collected with the model running 32 times and incrementing in steps of 0.003125 seconds from $t = 0$ *to* $t = 0.1$ seconds. The rms roughness was kept constant at 5 meters. The surface wave speed was kept constant at 1000 m/s. Figures 4.1 through Figs. 4.5 represent trial numbers 1, 8 , 16, 24, and 32 with t=0, t=0.02581, t=0.048387, t=0.074194, and t=0.1 seconds respectively. Observe the Bragg scatter by noting how the changes in the reflected rays (as time progresses) travel in distinct directions.

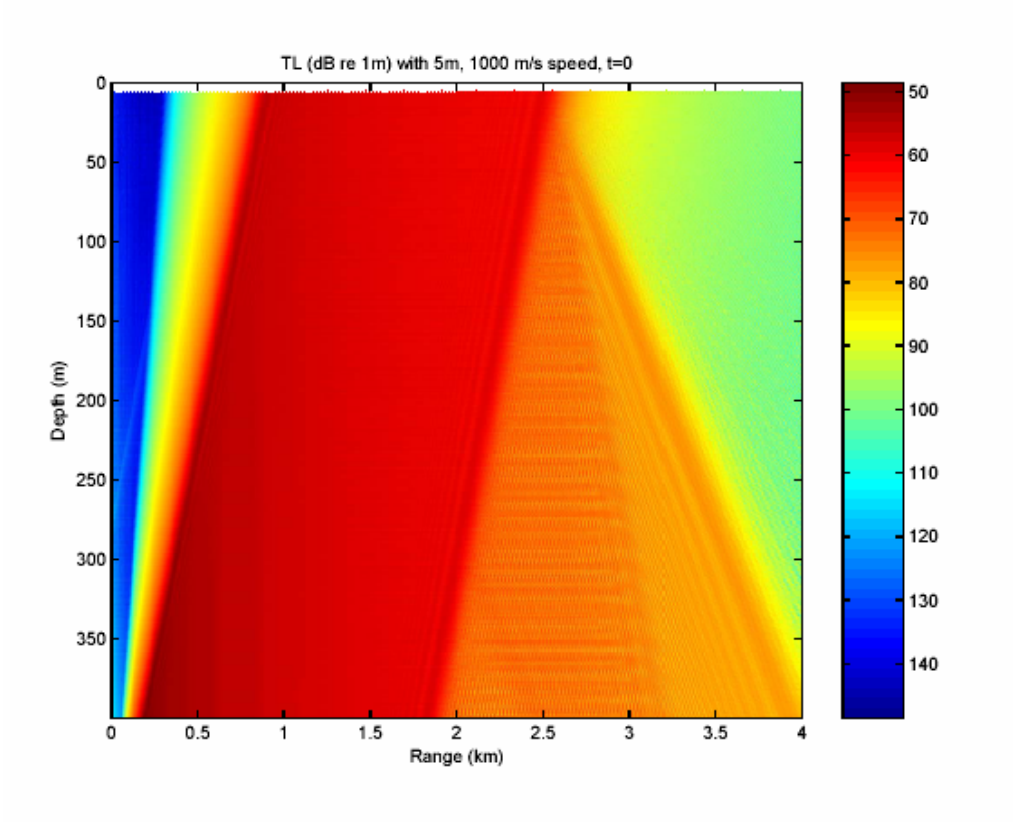

Figure 4.1 Trial #1, t=0

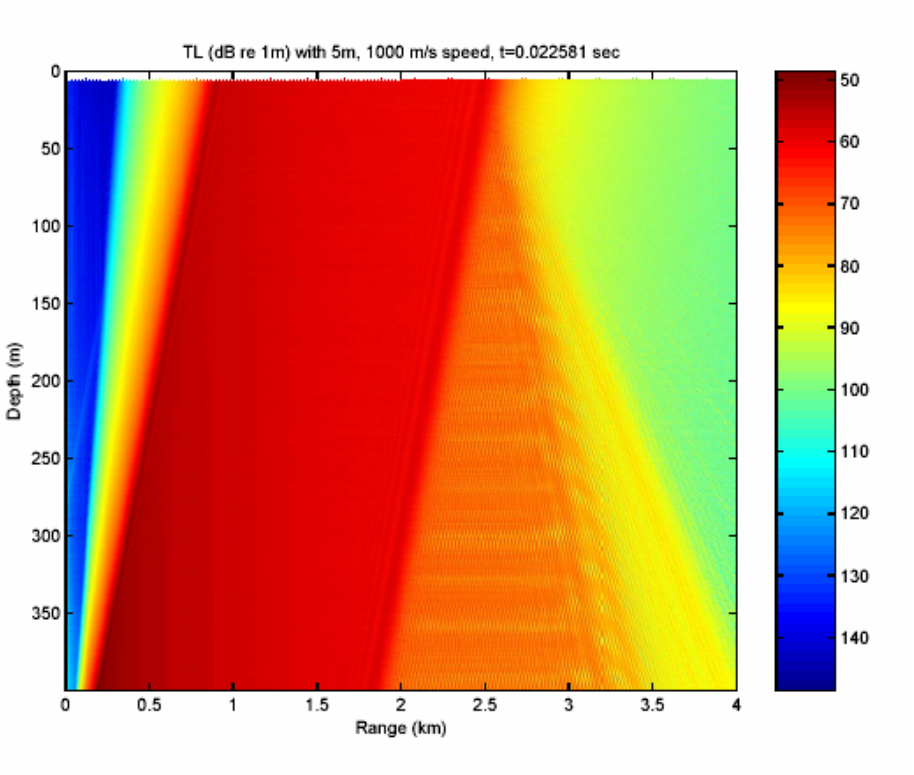

Figure 4.2 Trial #8, t=0.022581

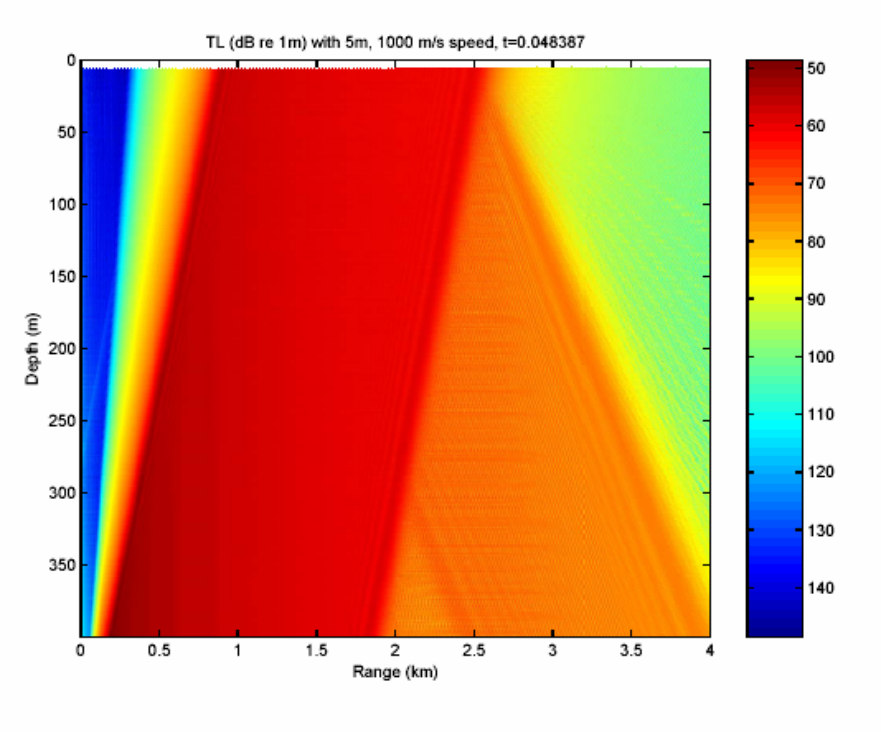

Figure 4.3 Trial #16, t=0.048387

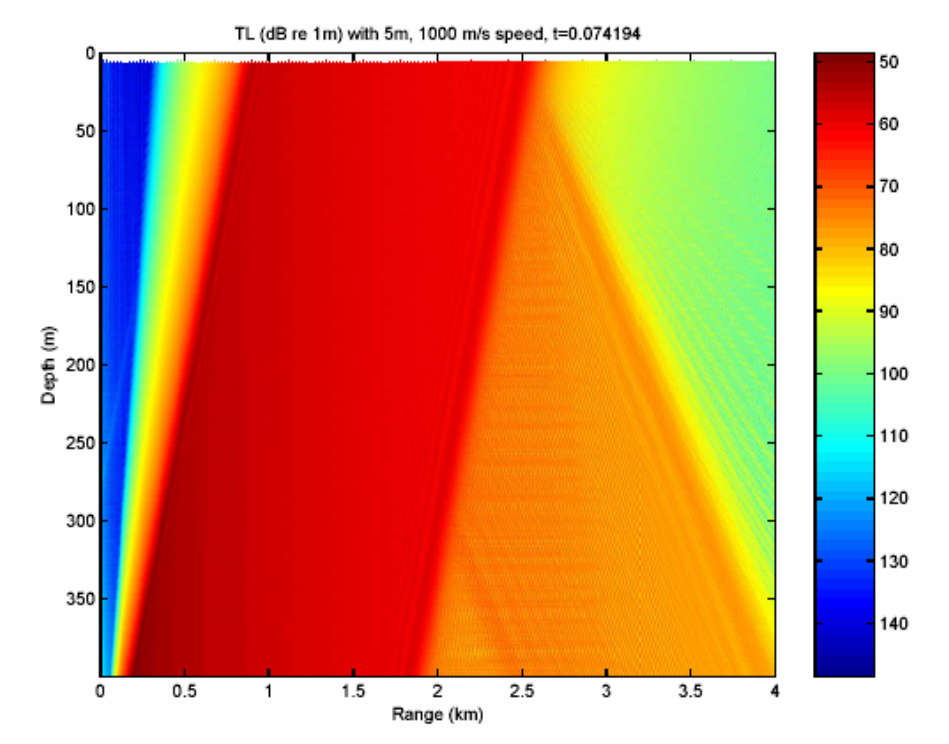

Figure 4.4 Trial #24, t=0.074194

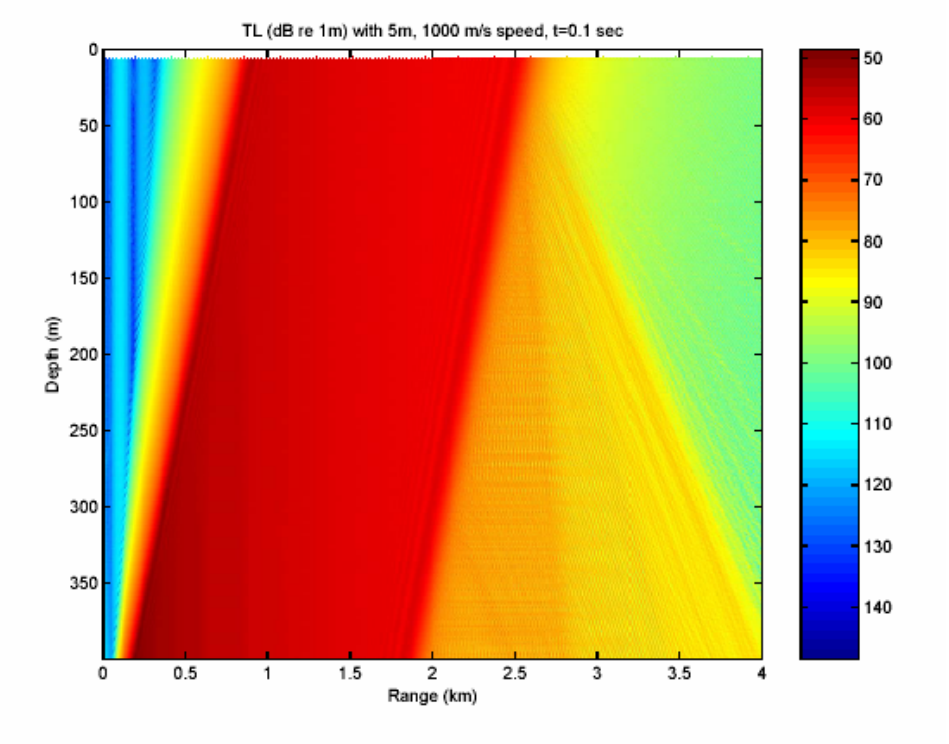

Figure 4.5 Trial #32, t=0.1

B. REALIZATION

Data was extracted at single ranges of 2.5 and 3.0 km. This produced pressure matrices in the MATLAB workspace as functions of depth and frequency. From these pressure matrices, data vectors were extracted at depths of 100, 150, 200, 250, 300, and 350 m. An inverse FFT followed by an FFT shift was performed on the data vectors and finally the absolute value was computed prior to displaying the results.

To automate the process a shell program was developed in MATLAB that cycles 128 times calling the MMPE update program and saving the wave speed and elapsed time, t, each cycle for use by the environmental propagator subroutine, ENVPROP1. The time t is incremented with the formula, t=(N-1) * Dt, where Dt is set to 0.002 seconds. The calculation for the surface displacement,

$$\eta(r) = A\sin\left[\frac{2\pi}{\lambda_w}(r + v_w t)\right], \tag{4.7}$$

is computed by ENVPROP1. When the program is run (approximately 8 hours at 2.2 G Hz processing speed) 128 bin files are generated.

Next, PEOUT1 and PEOUT2 were combined into one MATLAB program, PEOUT11FN, and treated as a function. A main program, PEOUMAIN, was developed which loops 128 times performing the computations as described previously and outputs the final plots. Figs 4.6 through 4.17 show the results with the frequency spectrum varying from + and – 150 Hz in 50 Hz steps.

C. EXAMINING RESULTS

According to the Bragg scatter conditions, there should be Doppler signatures at $\pm 50\,Hz$, $\pm 100\,Hz$, and potentially even a contribution at $\pm 150\,Hz$. The results in Figs 4.6 through 4.17 show energy predominately at $\pm 50\,Hz$, and $\pm 100\,Hz$, with a small amount of energy occurring at bins $\pm 150\,Hz$ in Figs 4.6, 4.8, 4.10, 4.12. 4.14, and 4.16 (all at a range of 2.5 km). Thus, the updated model has been verified effective at computing Doppler spread due to surface motion by using the exaggerated surface wave speed of 1000m/s.

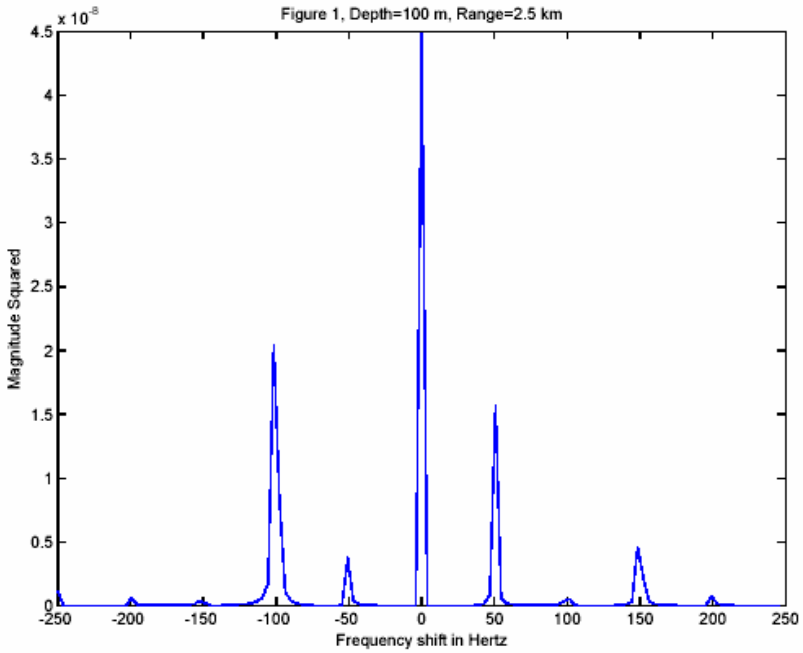

Figure 4.6 Frequency Spectra at a depth of 100m and range of 2.5 Km

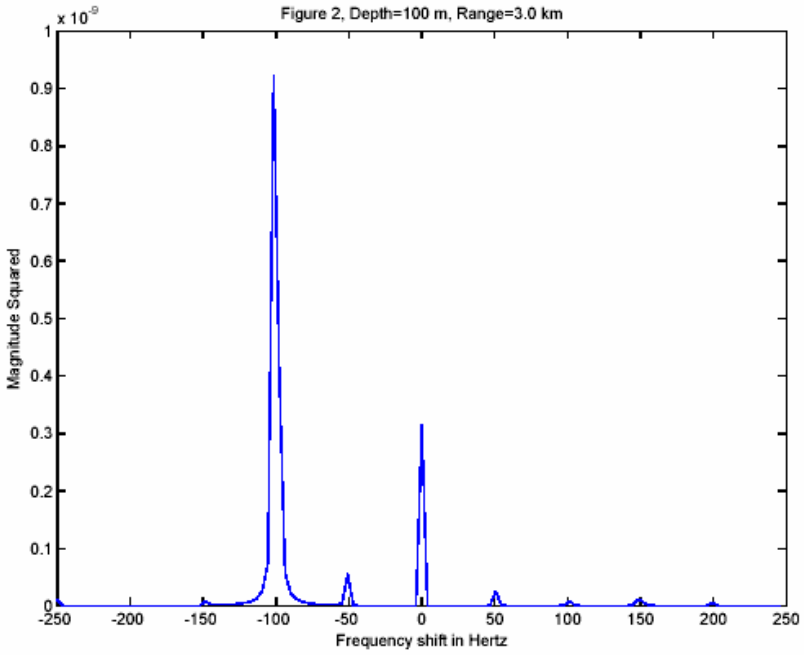

Figure 4.7 Frequency Spectra at a depth of 100m and range of 3.0 Km

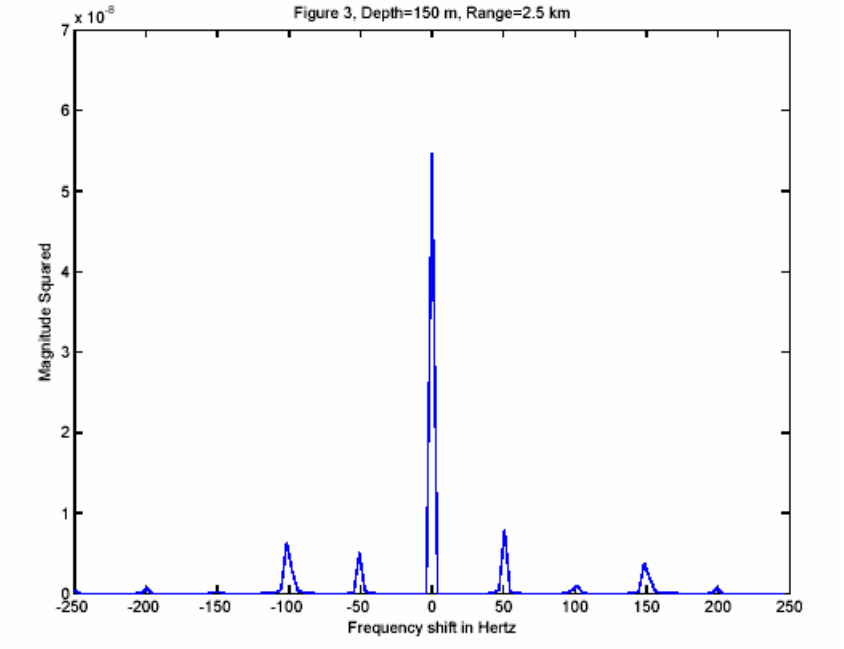

Figure 4.8 Frequency Spectra at a depth of 150m and range of 2.5 Km

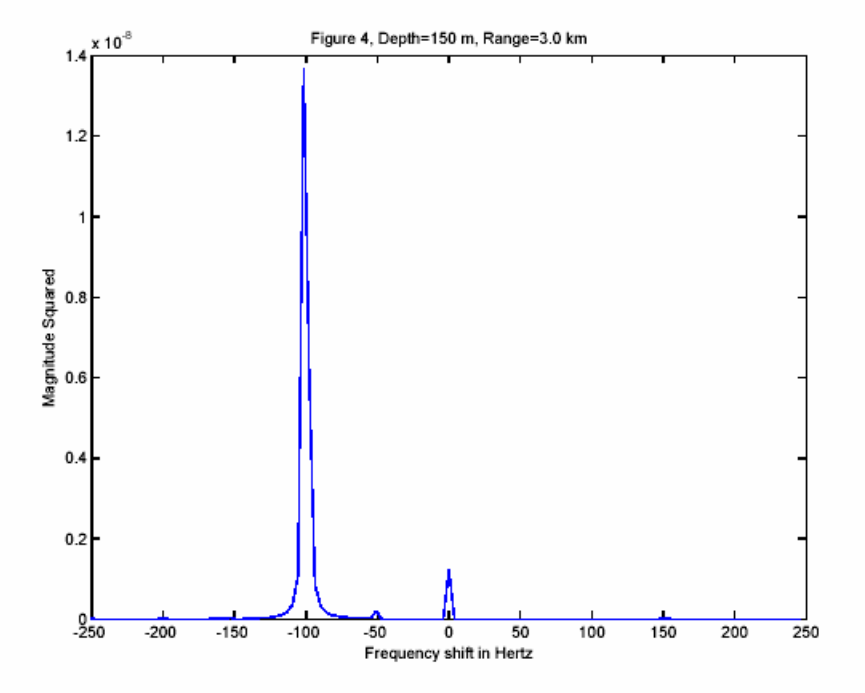

Figure 4.9 Frequency Spectra at a depth of 150m and range of 3.0 Km

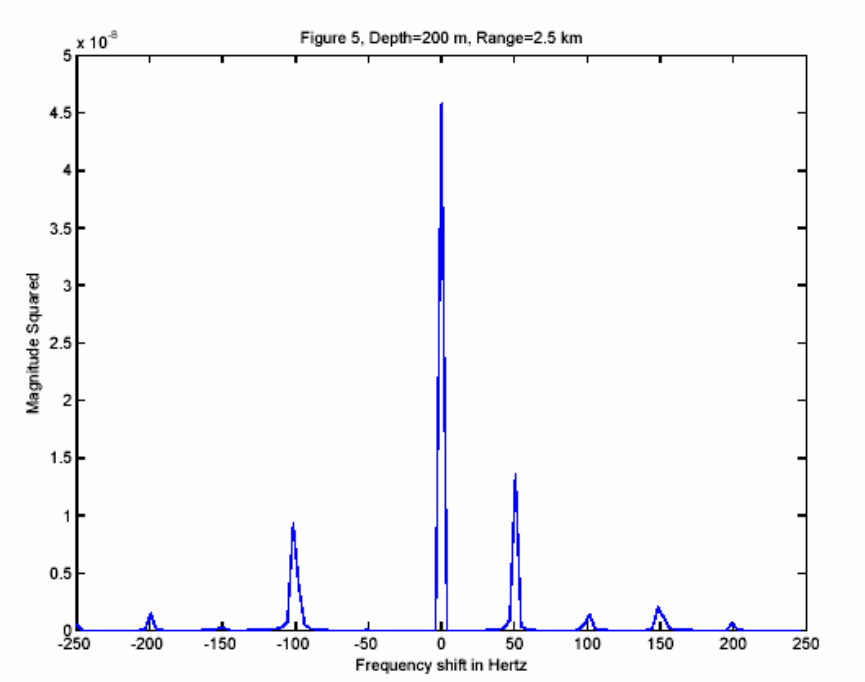

Figure 4.10 Frequency Spectra at a depth of 200m and range of 2.5 Km

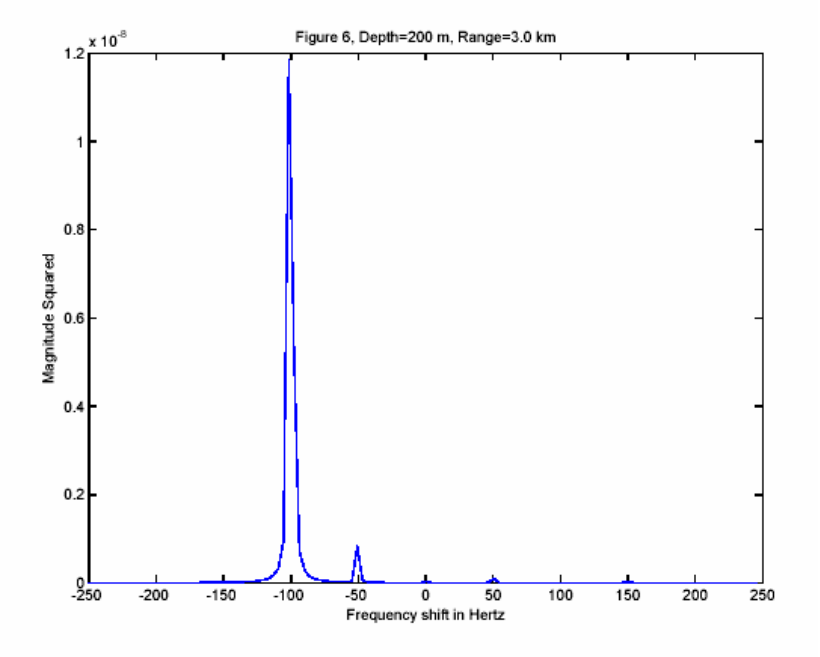

Figure 4.11 Frequency Spectra at a depth of 200m and range of 3.0 Km

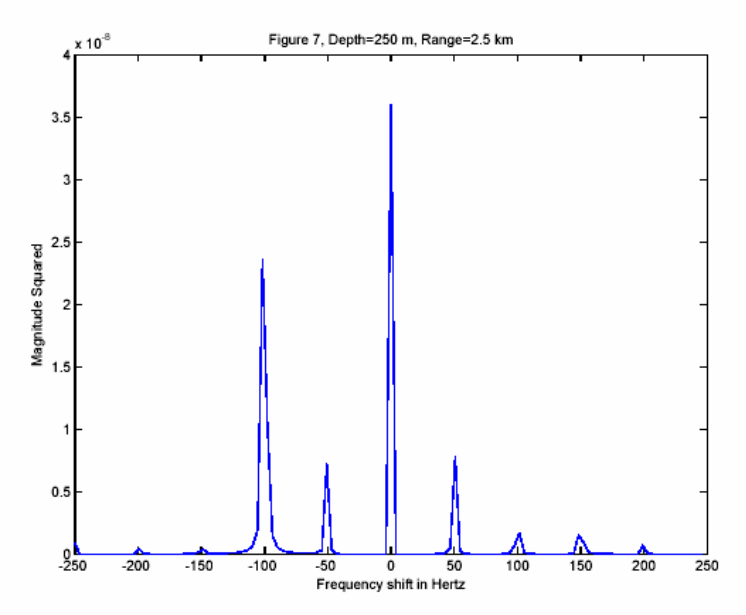

Figure 4.12 Frequency Spectra at a depth of 250m and range of 2.5 Km

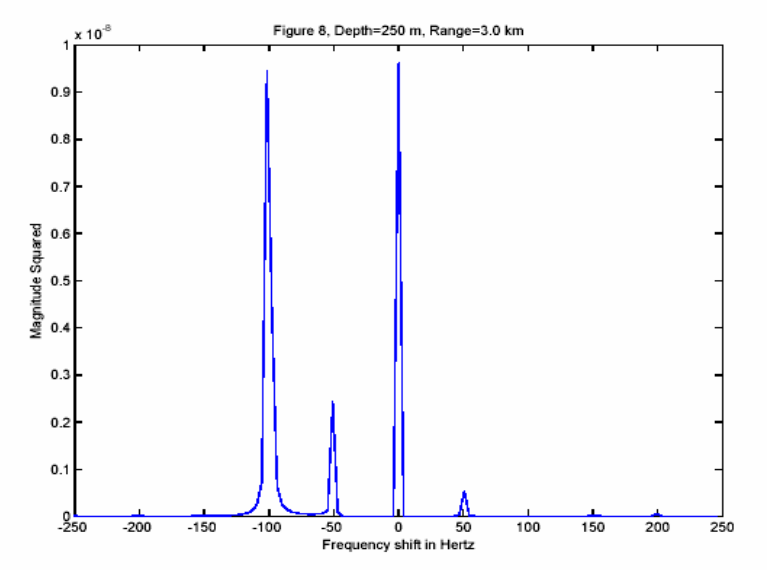

Figure 4.13 Frequency Spectra at a depth of 250m and range of 3.0 Km

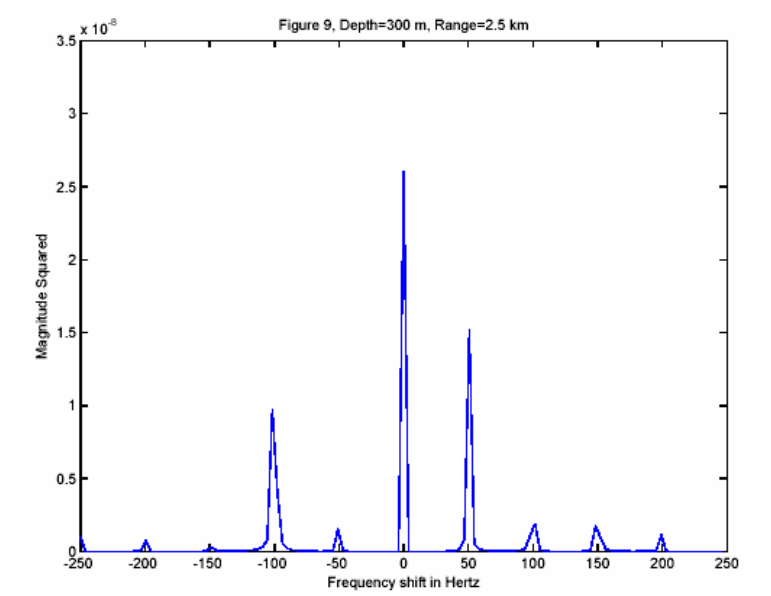

Figure 4.14 Frequency Spectra at a depth of 300m and range of 2.5 Km

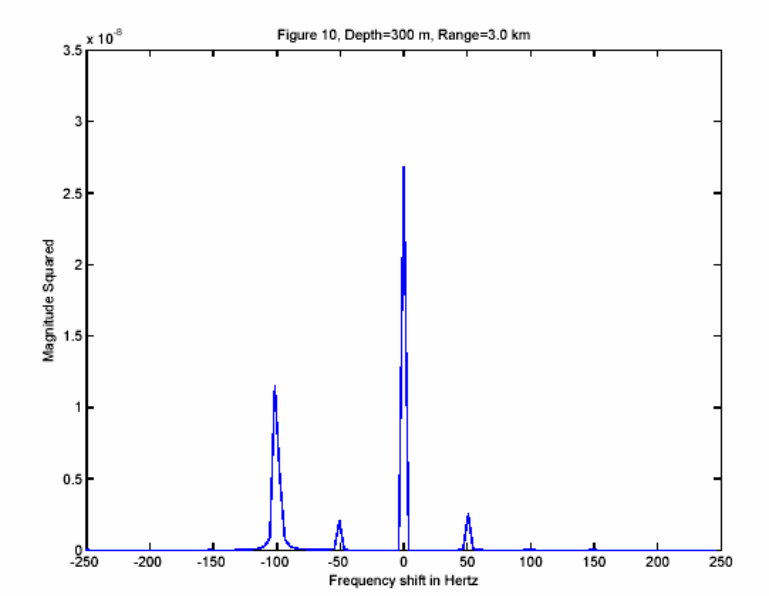

Figure 4.15 Frequency Spectra at a depth of 300m and range of 3.0 Km

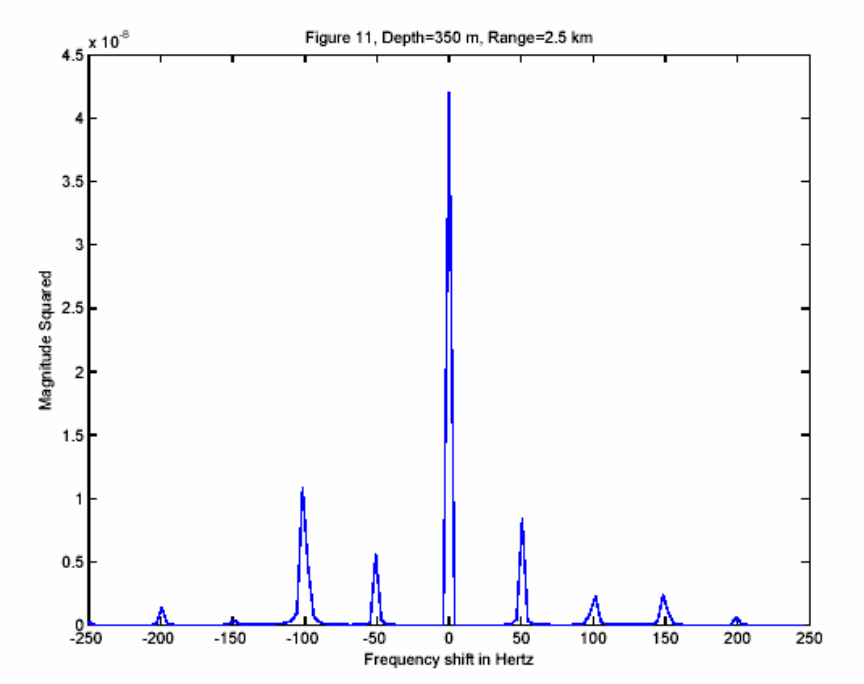

Figure 4.16 Frequency Spectra at a depth of 350m and range of 2.5 Km

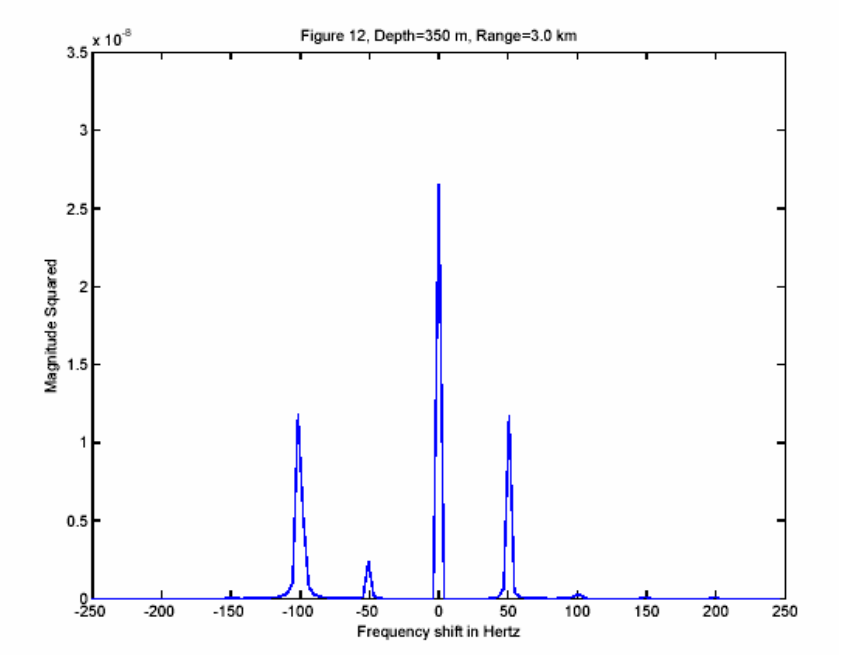

Figure 4.17 Frequency Spectra at a depth of 350m and range of 3.0 Km

The main program, PEOUTMAIN was modified to compute average spectra for ranges of 2.5 and 3.0 km over depths of 100, 150, 200, 150, 300, and 350 m. Figures 4.18 through 4.25 are the results. Figures 4.24 and 4.25 show spectra averaged over the six depths at ranges of 3.5 and 4.0 km respectively.

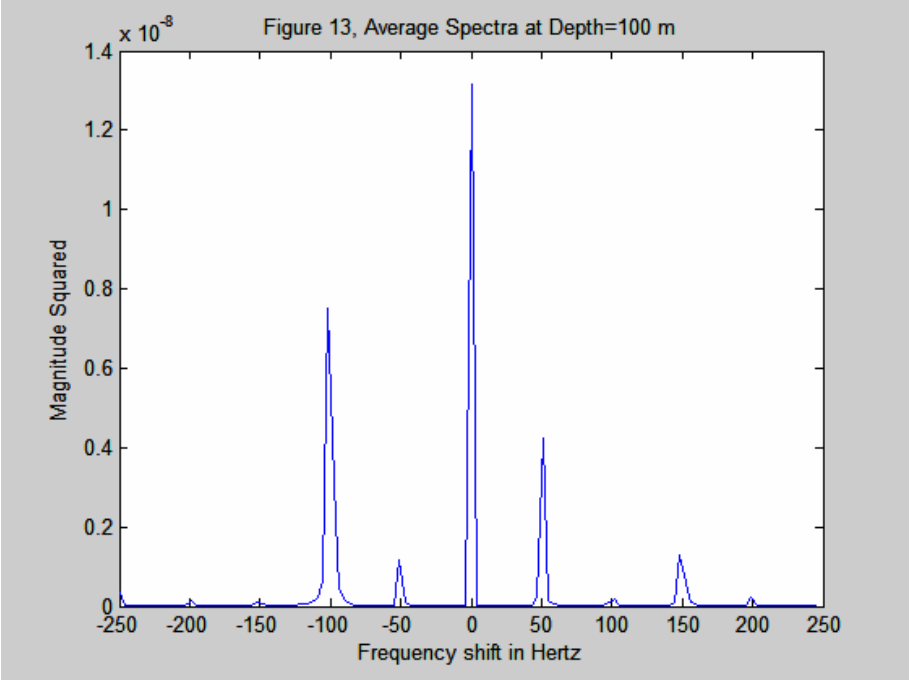

Figure 4.18 Average of Spectra at Ranges 2.5 and 3.0 km for Depth of 100 m

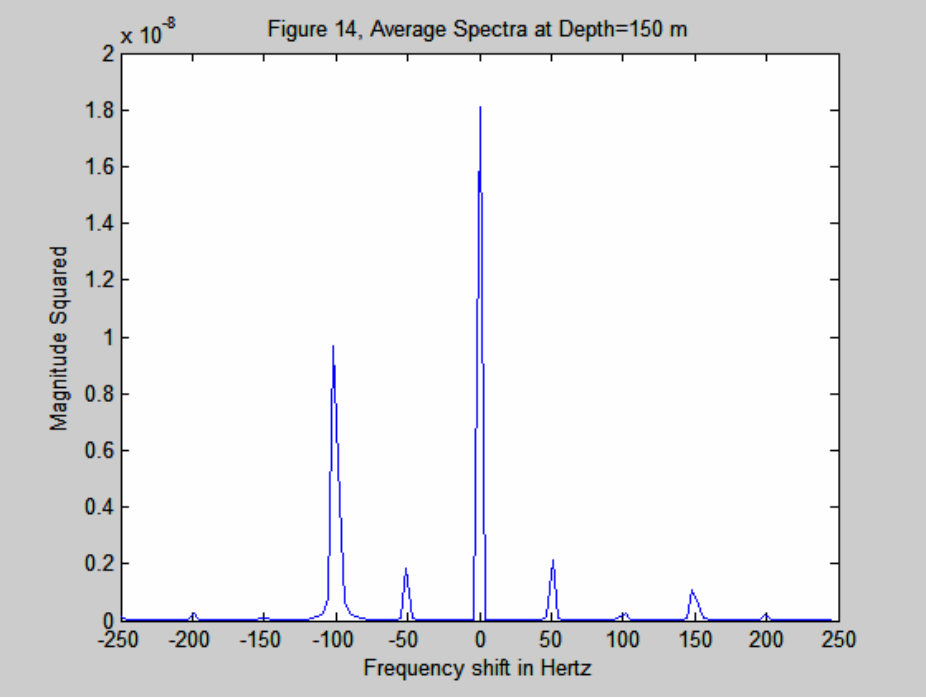

Figure 4.19 Average of Spectra at Ranges 2.5 and 3.0 km for Depth of 150 m

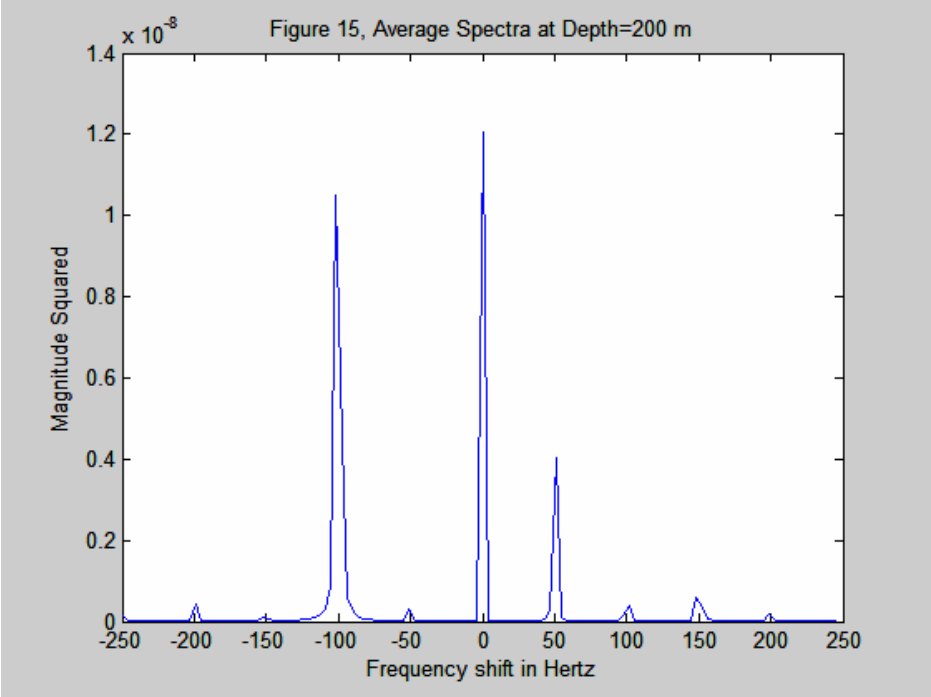

Figure 4.20 Average of Spectra at Ranges 2.5 and 3.0 km for Depth of 200 m

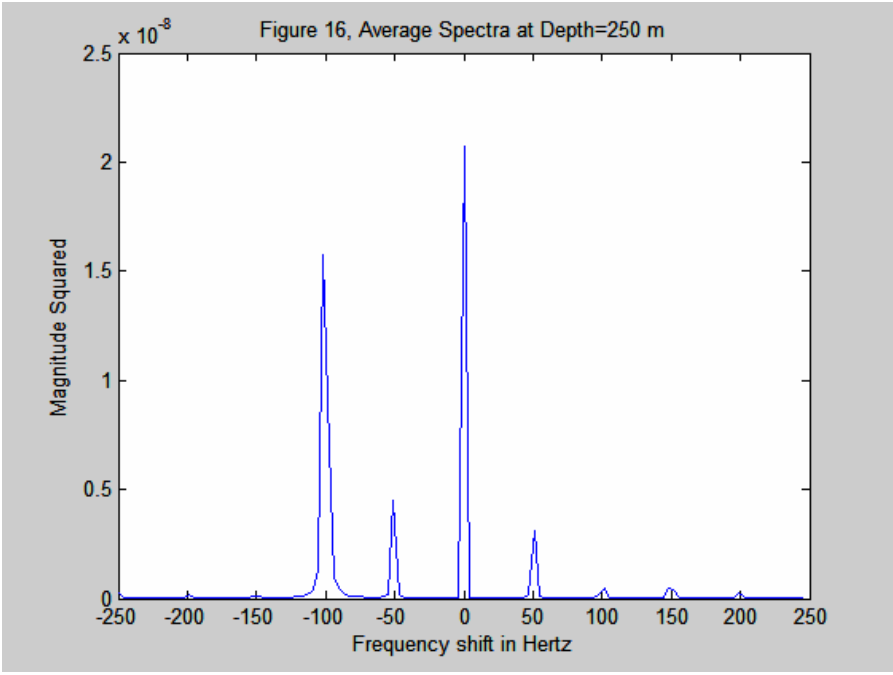

Figure 4.21 Average of Spectra at Ranges 2.5 and 3.0 km for Depth of 250 m

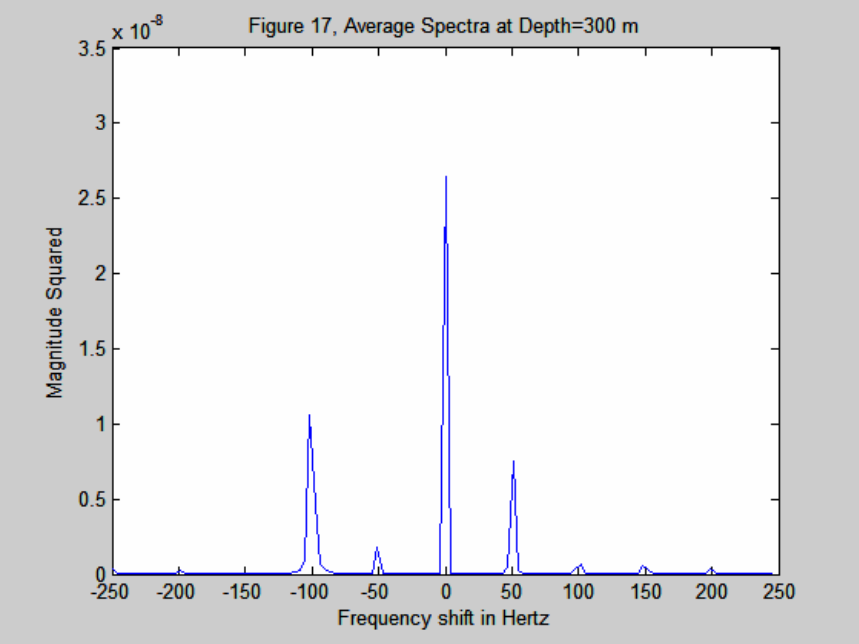

Figure 4.22 Average of Spectra at Ranges 2.5 and 3.0 km for Depth of 300 m

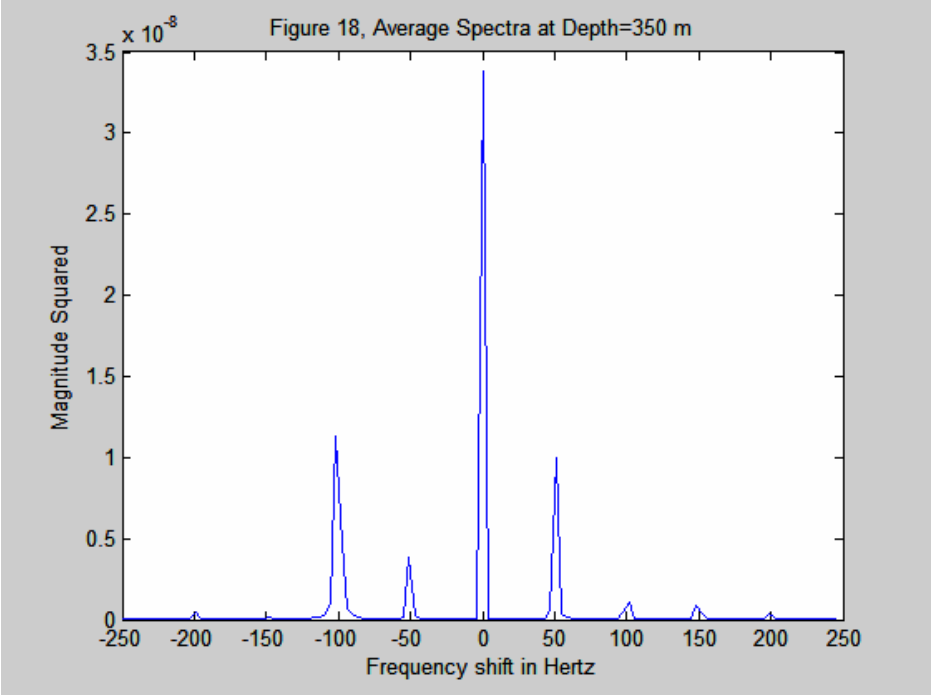

Figure 4.23 Average of Spectra at Ranges 2.5 and 3.0 km for Depth of 350 m

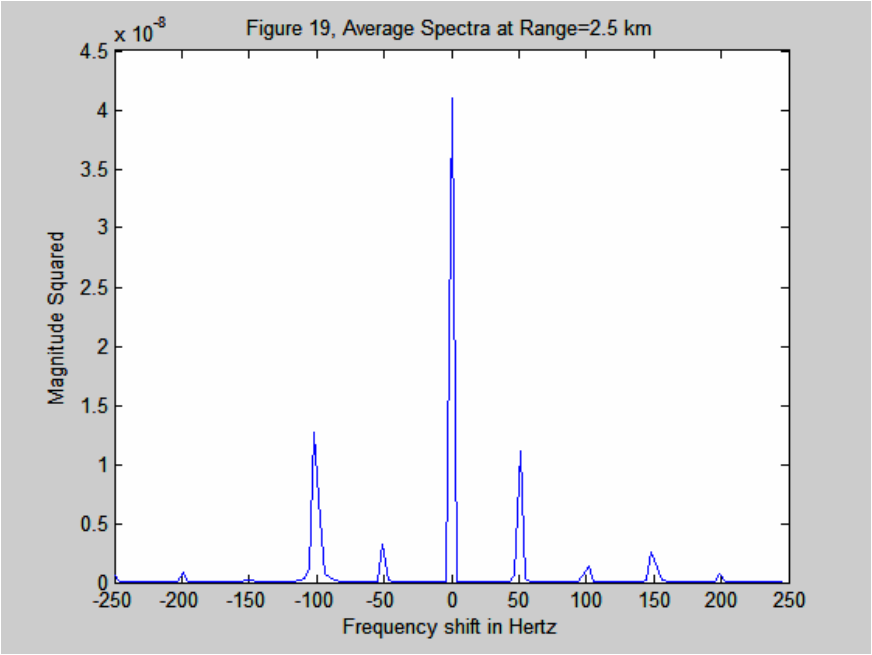

Figure 4.24 Average of Spectra at Depths 100-350 m at Range of 2.5 km

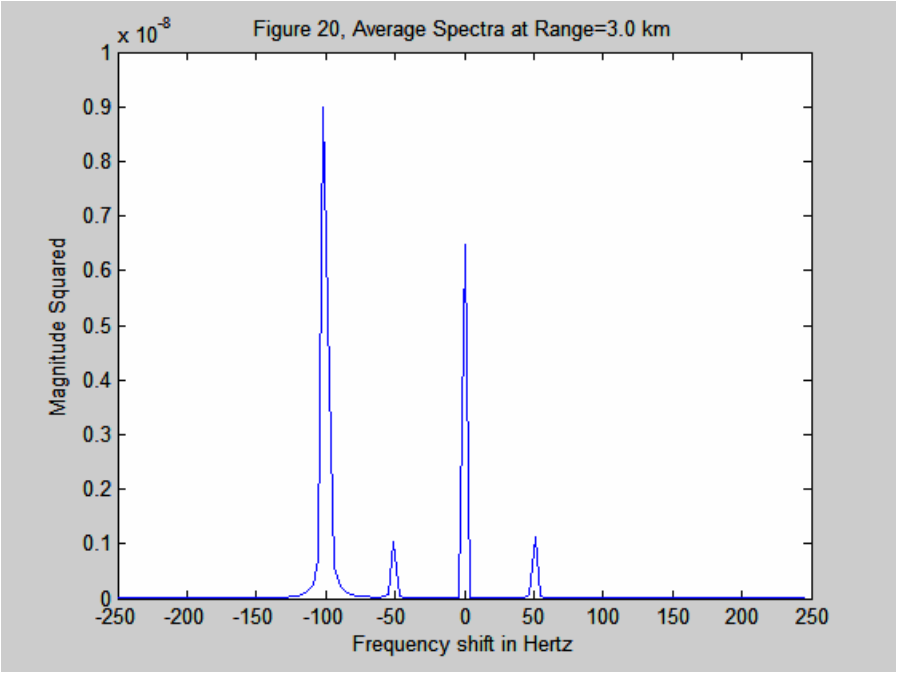

Figure 4.25 Average of Spectra at Depths 100-350 m at Range of 3.0 km

THIS PAGE INTENTIONALLY LEFT BLANK

V. ADVANCED MODELING ANALYSIS

In the previous chapter we examined the influence from a dynamically moving surface and verified that the updated model performs adequately. We now wish to examine the performance of the code in the presence of more realistic, complicated surfaces. To do that we shall consider a rough surface based on an empirical fetch-limited ocean wave spectrum and how such modeling compares with measured data.

A. PIERSON–MOSKOWITZ SPECTRUM

Pierson and Moskowitz (1964) analyzed wave observations in the North Atlantic and proposed a form of energy spectrum of fully developed waves for each wind speed. They assumed that if the wind blew steadily for a sufficiently long time and over a sufficiently large area, the waves would come into equilibrium. They calculated the surface wave spectra for various wind speeds and determined that the spectra were of the form

$$S(\omega) = \frac{\alpha g^2}{\omega^5} \exp\left[-\beta \left(\frac{\omega_0}{\omega} \right)^4 \right], \tag{5.1}$$

where $\omega = 2\pi f$, f is the surface wave frequency in Hertz, $\alpha = 8.1\,x\,10^{-3}$, $\beta = 0.74$, and $\omega_0 = g/U$, where U is the wind speed reported by weather ships at a height of 19.5 meters above the sea surface. Equation (5.1) is shown plotted in Fig. 5.1 with wind speeds from 15 to 20 m/s. Note the shift in peak response to slightly higher wave frequencies as the winds diminish.

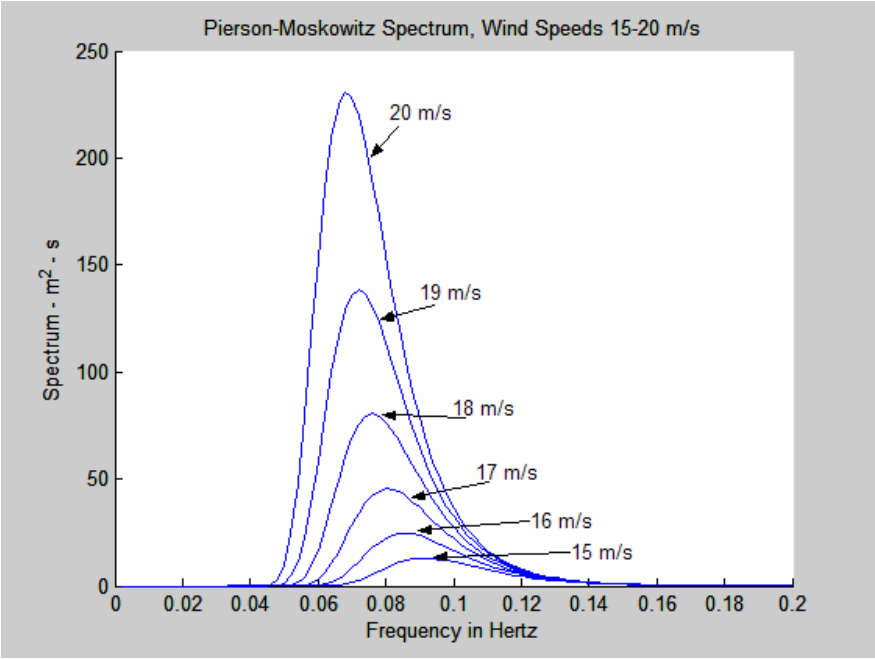

Figure 5.1 Pierson-Moskowitz Spectrum

B. JONSWAP SPECTRUM

Hasselmann et al. (1973) determined after analyzing data collected during the Joint North Sea Wave Observation Project (JONSWAP) conducted in 1973 that the wave spectrum is never fully developed. It was found that for all wind speeds, the energy spectrum for growing waves took on similar characteristics depending on the stage of development of the waves and that this was due to the effect of non-linear wave interactions. A wave spectrum was proposed of the following form

$$S(\omega) = \alpha g^2 \omega^{-5} \exp\left[-1.25\left(\frac{\omega}{\omega_p}\right)^{-4}\right]\gamma^{\delta}, \qquad (5.2)$$

where δ is the peak enhancement factor,

$$\delta = \exp\left[-\frac{(\omega-\omega_p)^2}{2\sigma_0^2\,\omega_p^2}\right], \qquad (5.3)$$

with $\gamma = 3.3,\quad \sigma_0 = 0.07$ *for* $\omega \le \omega_p$, *and* $\sigma_0 = 0.09$ *for* $\omega > \omega_p$, while α is a function of fetch, *X*, and wind speed, *U*. Fetch is the distance from the lee shore or the distance over which the wind blows with a constant velocity, such that

$$\alpha = 0.076\left(\frac{gX}{U}\right)^{-0.22}. \tag{5.4}$$

The peak frequency is calculated by

$$\omega_p = 7\pi\left(\frac{g}{U}\right)\left(\frac{gX}{U^2}\right)^{-0.33}. \tag{5.5}$$

Equation (5.2) is plotted in Fig. 5.2 with a constant fetch of 7.5 km and wind speeds varying from 10 to 30 m/s. Note how the peak frequencies diminish in amplitude as the wind speed diminishes and how the diminishing peaks increase in frequency. Figure 5.3 is a plot of (5.2) with wind speed constant at 10 m/s and the fetch varying from 4 to 12 km. Note further how the amplitude of the peak frequencies increases with increasing fetch. Thus one can conclude that in coastal regions, the wind acts on a limited fetch with the result that the sea swell components may be less than what otherwise might occur in an open ocean environment and occur at higher frequency.

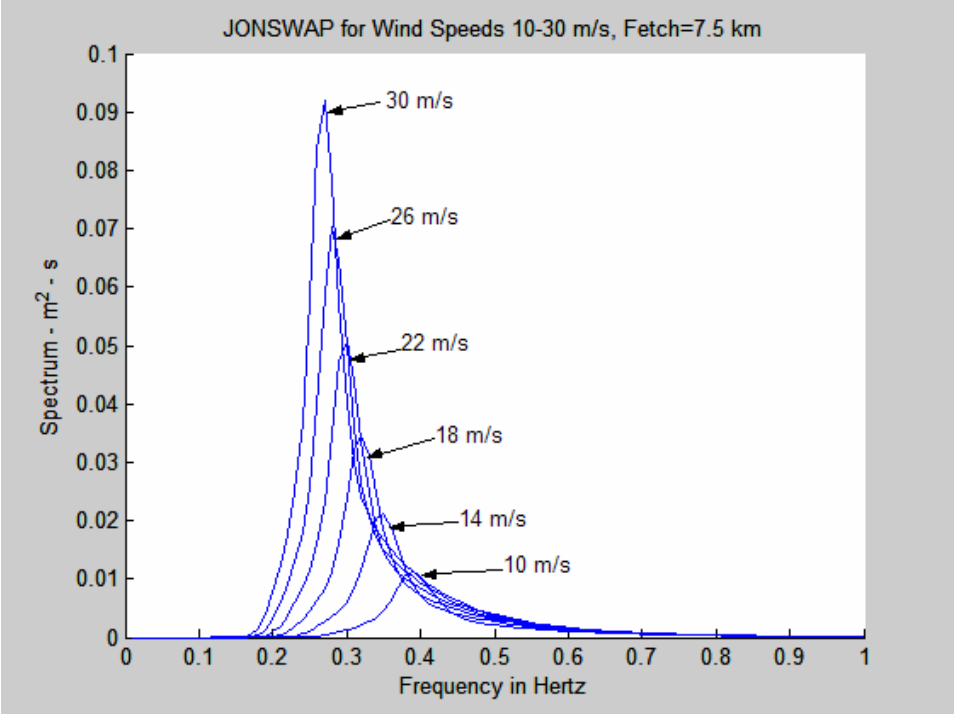

Figure 5.2 JONSWAP Spectrum with Varying Wind Speed and Constant Fetch

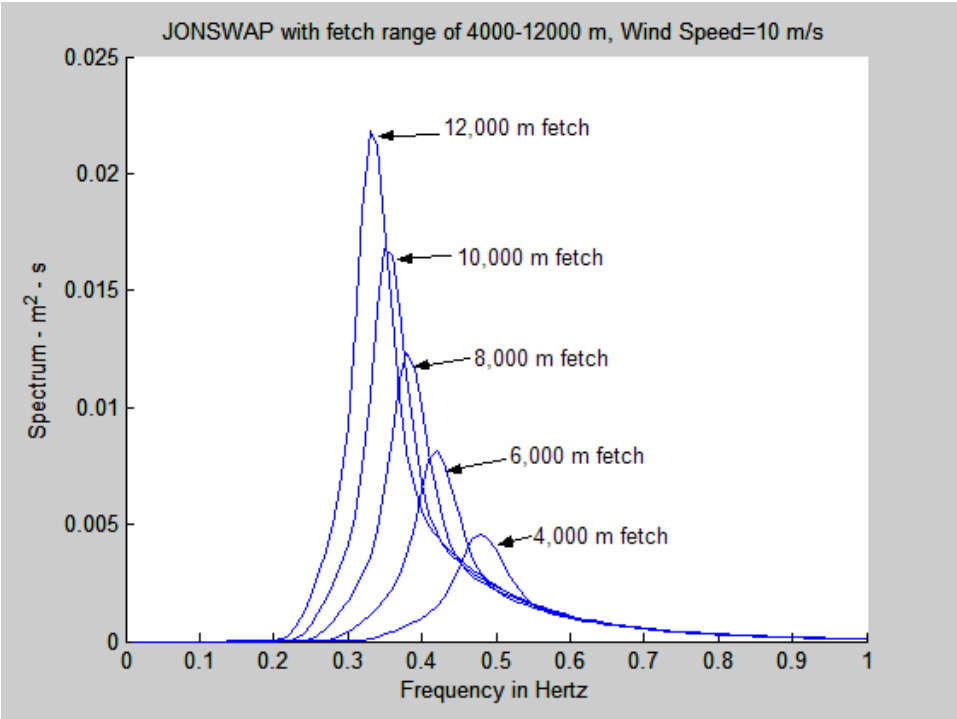

Figure 5.3 JONSWAP Spectrum with Varying Fetch and Constant Wind Speed

C. HFA97 EXPERIMENT

In September 1997, a high frequency acoustic experiment (HFA97) was conducted in a central region of the Delaware Bay. The intent of the HFA97 experiment was to measure cause and effect between the ocean environment and acoustic propagation. Two stable tripods, each having an acoustic source and three receiving hydrophones, were placed in 15 m of water separated by 387 m. On each tripod the source was located 3.125 m above the sea floor and the three receiving hydrophones were located at 0.33, 1.33 and 2.18 m. See Fig. 5.4 for details about the experimental setup.

A broadband chirp signal in the frequency range from 1-18 kHz was transmitted every 0.345 seconds for an interval in one case of 5 seconds repeated every 10 minutes and in a second case for an interval of 40 seconds repeated every hour.

In prior analysis of HFA97 data, remotely received signals across the three hydrophones were used with a beamforming technique to calculate signal arrival angle as a function of arrival time (Badiey, et al, 2000). By considering the geometry of the HFA97 experimental setup, the resulting beamformed plots can be used to easily distinguish that portion of the received signal corresponding to single surface reflected wave paths, as shown in Fig. 5.5.

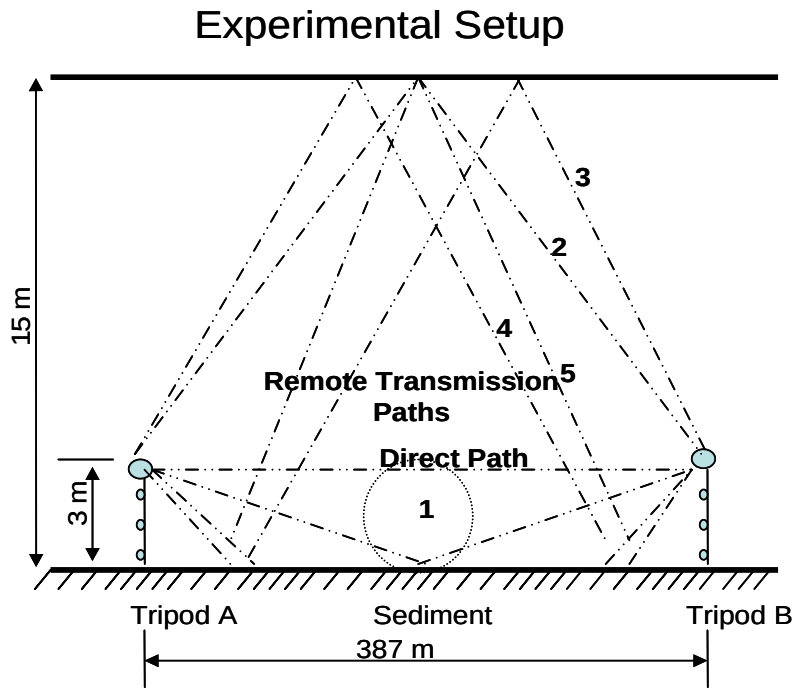

Figure 5.4 HFA97 Experimental Setup, numbers 2, 3, 4, and 5 represent single surface reflected ray paths (After Ref. [Heitsenrether, Badiey, 2004]).

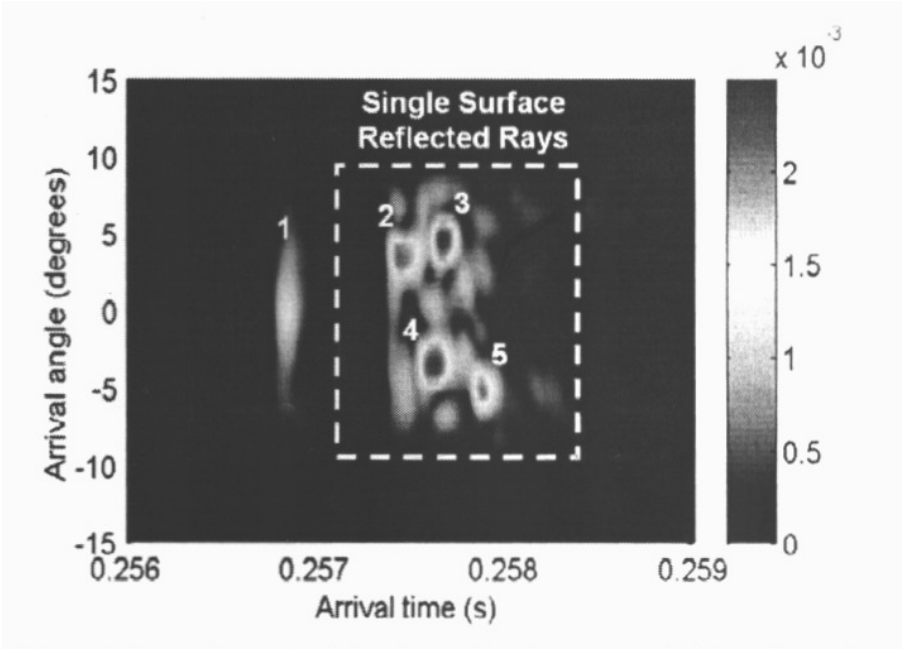

Figure 5.5 Received signal arrival angle versus arrival time for a calm period. Single surface reflected ray paths are easily distinguished in the signal (From Ref. [Heitsenrether, Badiey, 2004]).

D. IMPLEMENTATION OF JONSWAP INTO MMPE MODEL

A sea surface deviation wavenumber spectrum, *W(k)* obtained from the JONSWAP wave spectrum, Equation (5.2), has the form

$$W(k) = S(\omega)\frac{d\omega}{dk} \ . \tag{5.6}$$

With the wave dispersion relationship $\omega = \sqrt{kg}$,

$$\frac{d\omega}{dk} = \frac{1}{2}\sqrt{\frac{g}{k}} \quad , \tag{5.7}$$

where *k* is the wavenumber of ocean waves. From Equations (5.2) through (5.7), the sea surface wavenumber spectrum can be shown to have the form

$$W(k) = \frac{\frac{1}{2}\sqrt{\frac{g}{k}}\ \alpha\, g^2\,(kg)^{-\frac{5}{2}}}{\frac{1}{2}\alpha\, k^{-3}} \exp\left[-\frac{5}{4}\ \omega_p{}^4\,(kg)^{-2}\right](3.3)^{\delta} \ . \tag{5.8}$$

From the wavenumber spectrum (5.8), code was developed for implementation into the rough surface forward scatter subroutine, ZSGEN, of the MMPE. Recall from Section III that ZSGEN calculates a roughness spectrum that serves as an input to ENVPROP for calculating the image ocean potential function. The changes to the ZSGEN program include the swapping of the one dimensional rough surface wave number spectrum calculation with the JONSWAP sea surface wavenumber spectrum calculation (5.8). The input parameters were selected from the setup in Figure 5.4 and include a source depth of 12 m, a maximum range of 0.387 km, and a water depth of 15 m. An isovelocity sound speed of 1500 m/s was selected, with sea bottom sound speed of 1650 m/s, and sea bottom density of 1.9 g/cc. A relatively high sea bottom attenuation of

0.5 db/km/Hz was chosen so as reduce scatter from the sea floor. A fetch distance of 7.5 km was input to the model as an estimate of actual conditions during HFA97. The sound source inputs included a center frequency of 9 kHz, a bandwidth of 16 kHz, and 256 frequencies selected for processing.

The model was run for various wind speeds. Figures 5.6 through 5.9 are the results for wind speeds of 1, 5, 10, and 15 m/s. When comparing these figures with Fig. 5.5 the similarities between the model and the empirical data are apparent. Note the dispersion of energy with the surface reflected paths as the wind speed increases and how the direct path is unaffected.

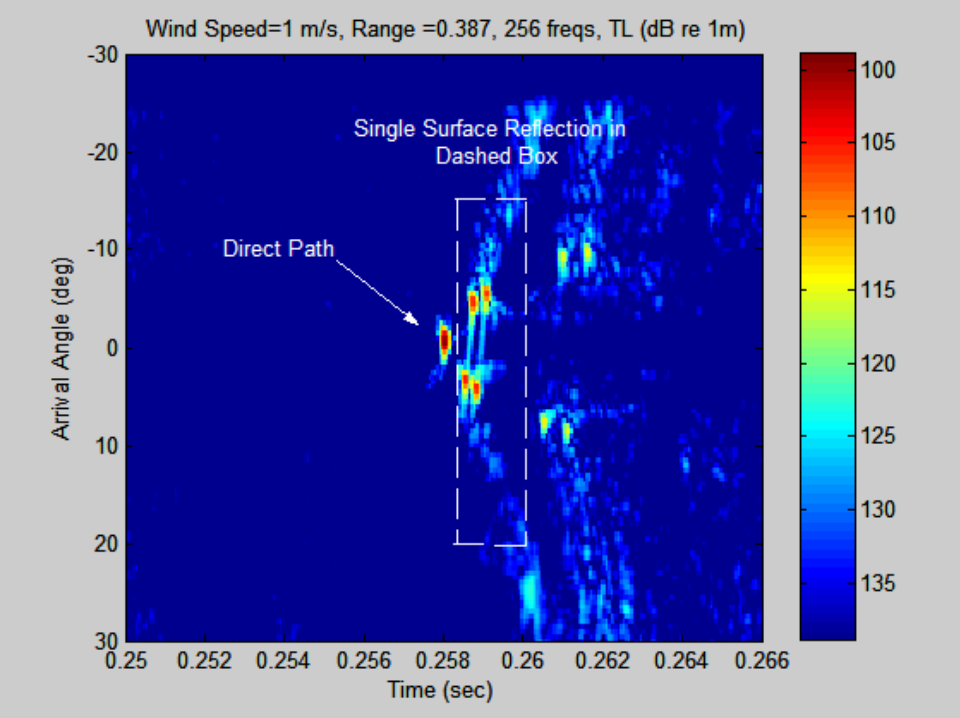

Figure 5.6 MMPE results of arrival angle versus arrival time for a wind speed of 1 m/s.

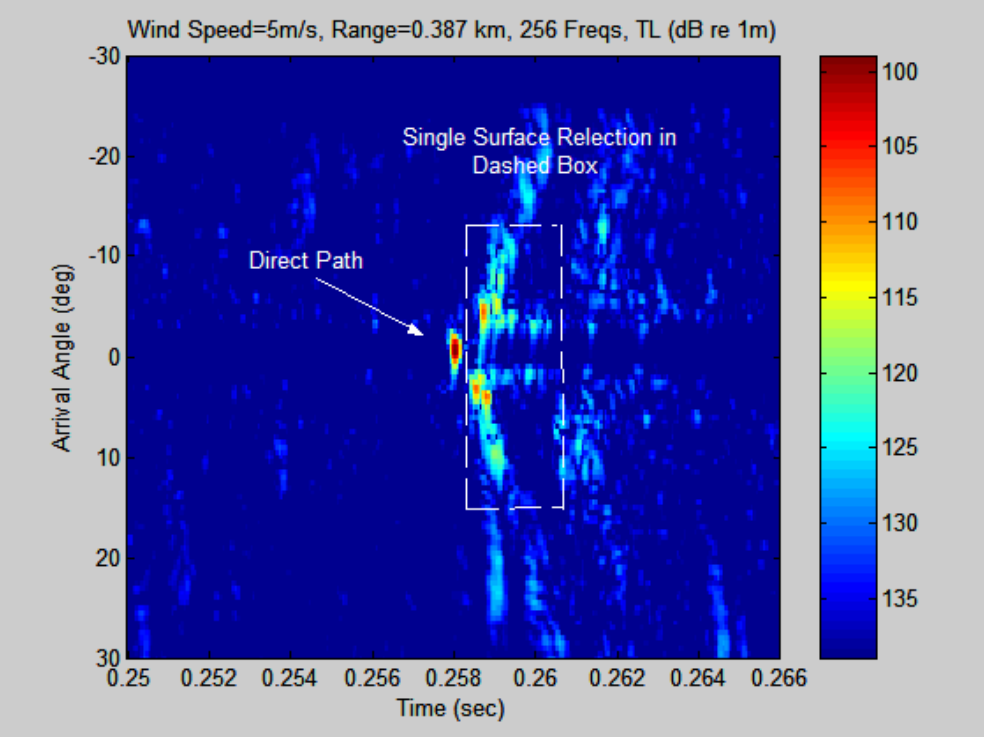

Figure 5.7 MMPE results of arrival angle versus arrival time for a wind speed of 5 m/s

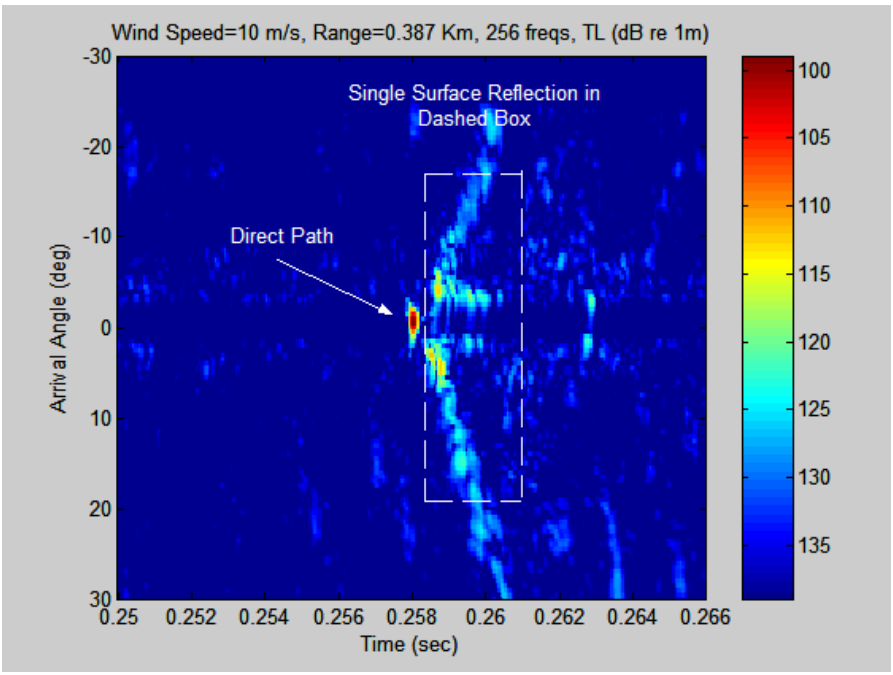

Figure 5.8 MMPE results of arrival angle versus arrival time for a wind speed of 10 m/s.

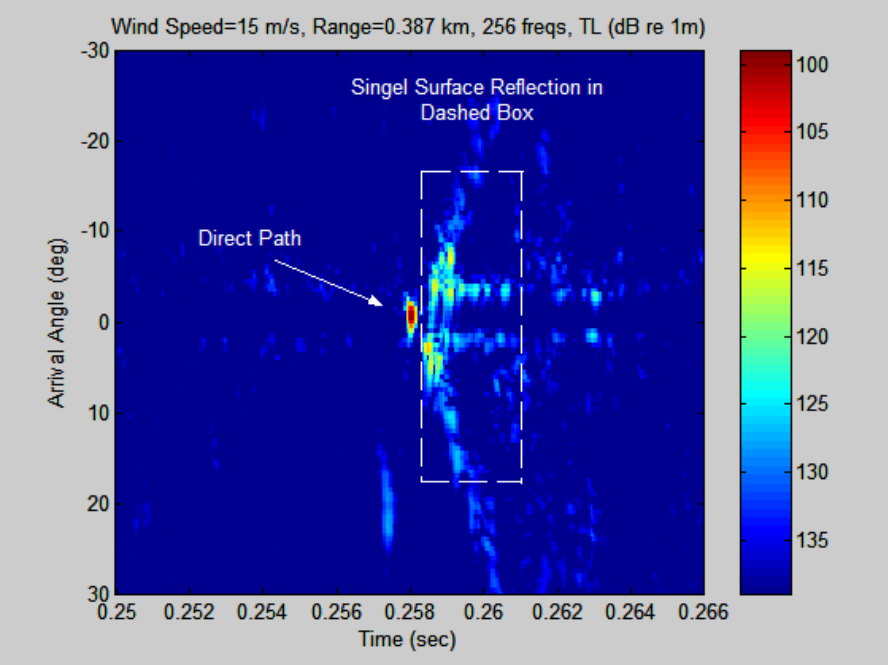

Figure 5.9 MMPE results of arrival angle versus arrival time for a wind speed of 15 m/s.

E. COMPUTING STANDARD DEVIATION OF ARRIVAL TIME AND ARRIVAL ANGLE

Two MATLAB programs were written for calculating the standard deviation of arrival angle and arrival time (see Appendix A for details of MATLAB code). For both algorithms, a narrow window or slice is sampled from the single surface return transmission loss pressure data for positive angles from 0 to 39.5 degrees and time width of 0.36 msecs. The minimum transmission loss value within the window is found and established as a reference point. Next, the data is sorted into twelve bins of transmission loss data each of 1 dB difference referenced to the minimum transmission loss value. The data in the 12 bins are next weighted by values of 32, 25, 20, 16, 13, 10, 8, 6, 5, 4, 3, and 3. An emphasis weighting value is added to the angle of arrival algorithm and operates on the higher transmission loss values. The emphasis adds linearity at the higher wind speeds

Measuring dispersion within a window or slice that contains data represented by position and magnitude, both of which are changing (dispersing) as the wind speed increases, is a challenging task. Various combinations involving window sizes, number of thresholds, threshold levels, and various weighting associated with each threshold were examined while trying to maintain a rational basis for the algorithms. Although not exact, the algorithms are considered a good approximation with the results shown in Figs. 5.10 and 5.11 being optimum when compared to HFA97 measured data results shown in Figs. 5.12 and 5.13.

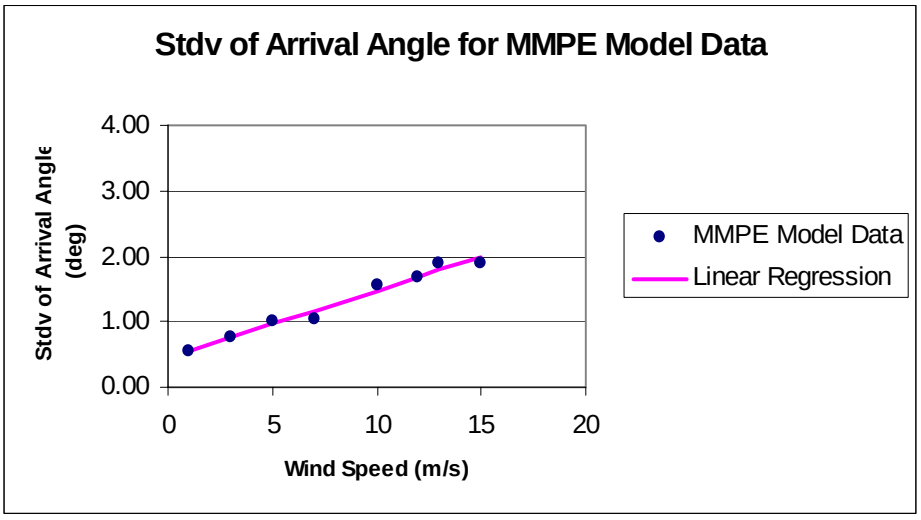

Figure 5.10 Standard Deviation of Arrival Angle vs. Wind Speed for MMPE Model Data

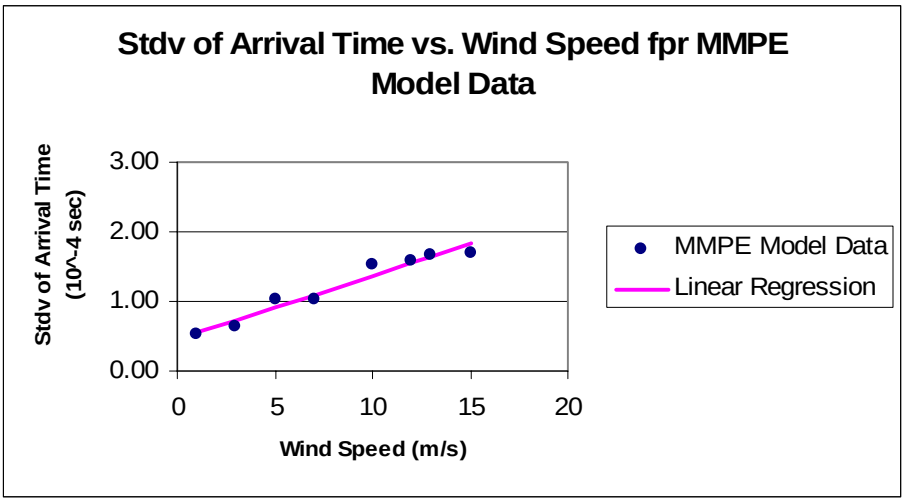

Figure 5.11 Standard Deviation of Arrival Time vs. Wind Speed for MMPE Model Data

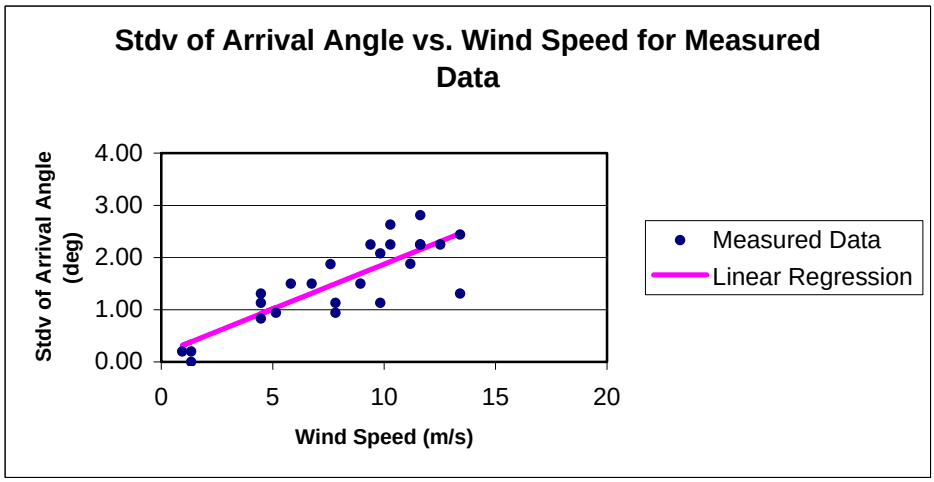

Figure 5.12 Standard Deviation of Arrival Angle vs. Wind Speed for Measured HFA97 data (After Ref. [Heitsenrether, Badiey, 2004]).

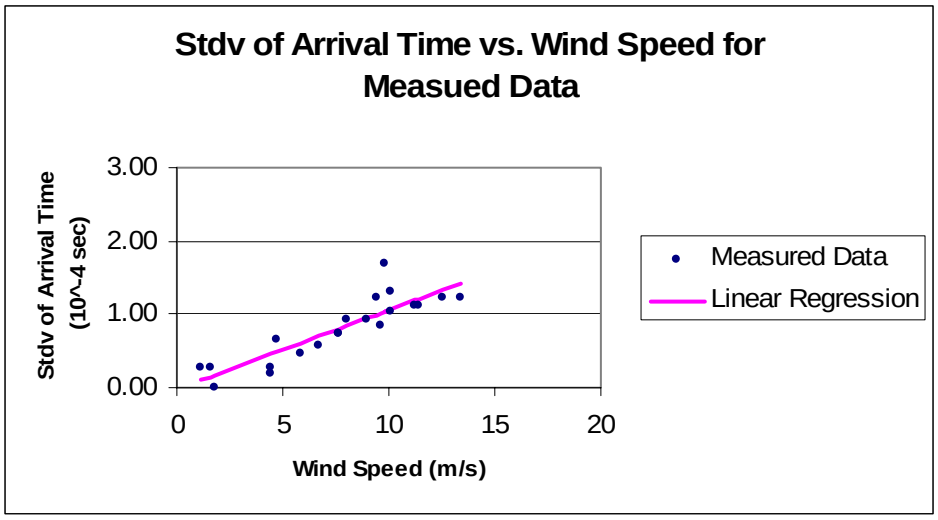

Figure 5.13 Standard Deviation of Arrival Time vs. Wind Speed for Measured HFA97 data (After Ref. [Heitsenrether, Badiey, 2004]).

Figures 5.14 and 5.15 compare regression analysis of measured data with modeled data for both arrival angle and arrival time (see Appendix B for details about regression statistics results). What can be gathered from the regression analysis is not only that acoustical energy dispersion increases with increasing wind speed, but also how the steepness of the slope of measured data and modeled data relates to the rate of acoustical energy dispersion. Thus, the MMPE model is predicting slightly lower energy dispersion rates when compared to an analysis of measured data. Note, however, that the MATLAB algorithms that compute the MMPE data arrival angle and arrival time statistics are considered approximations. Also, the window or slice of data that the algorithm examines may include a small portion of other acoustic energy besides reflection from just a single surface bounce.

Another model employed as a combination of an empirical sea surface model and a Gaussian beam tracing model (BELLHOP), termed the BELLHOP/JONSWAP model, was compared with measured data from the HFA97 experiment (Heitsenrether, Badiey, 2004). Figures 5.16 and 5.17 show results of the BELLHOP/JONSWAP model with input parameters taken from the HFA97 experiment.

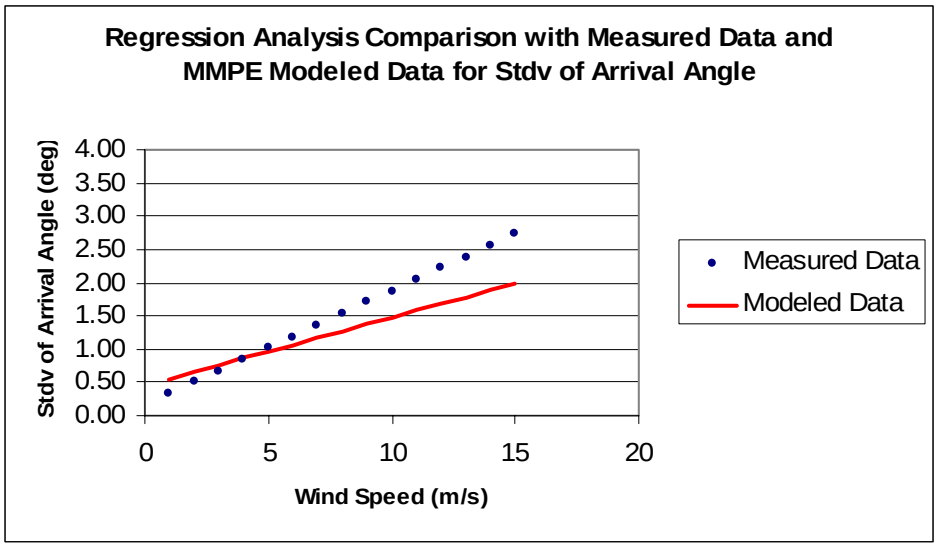

Figure 5.14 Regression Analysis Comparing Standard Deviation of Arrival Angle vs. Wind Speed for Measured and Modeled Data

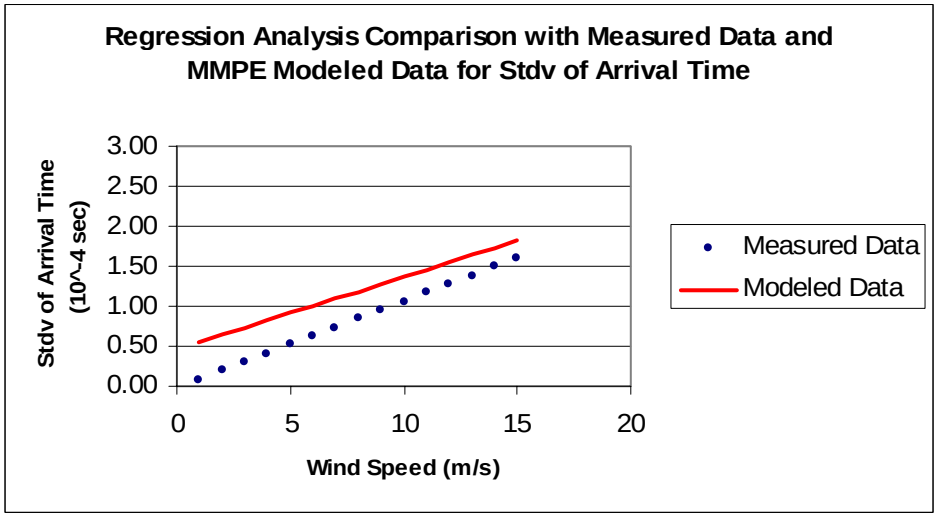

Figure 5.15 Regression Analysis Comparing Standard Deviation of Arrival Time vs. Wind Speed for Measured and Modeled Data

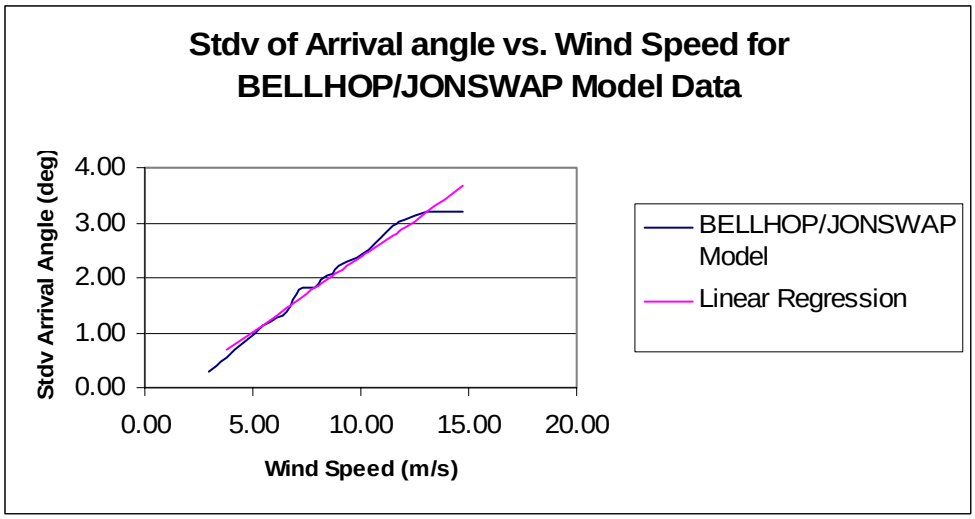

Figure 5.16 Standard Deviation of Arrival Angle vs. Wind Speed for BELLHOP/JONSWAP Model data (After Ref. [Heitsenrether, Badiey, 2004]).

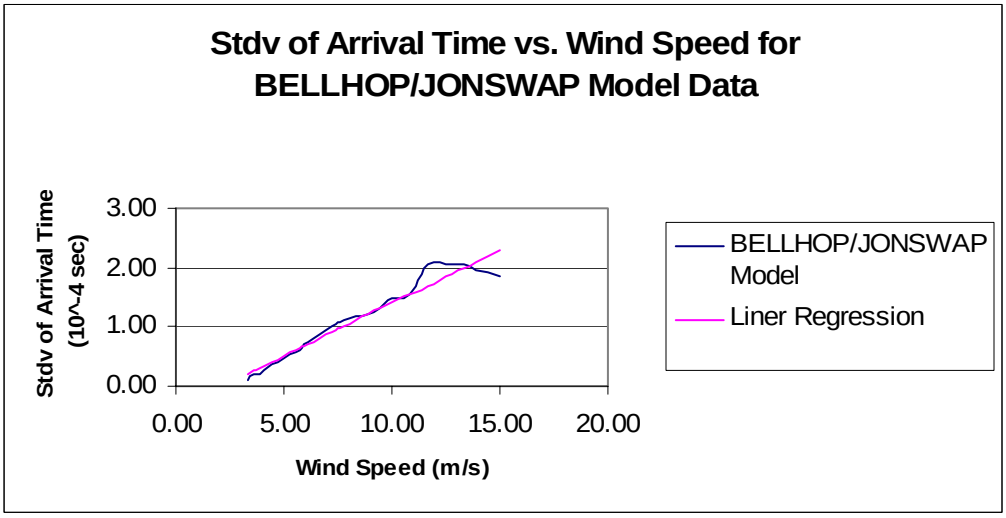

Figure 5.17 Standard Deviation of Arrival Time vs. Wind Speed for BELLHOP/JONSWAP Model data (After Ref. [Heitsenrether, Badiey, 2004]).

Finally, Figures 5.18 and 5.19 show a regression analysis comparison of the BELLHOP/JONSWAP model, measured data from the HFA97 experiment, and the MMPE model for both the standard deviation of arrival angle vs. wind speed, and the standard deviation of arrival time vs. wind speed. By examining the slopes of the three curves it is interesting to note how the BELLHOP/JONSWAP model is predicting a slightly greater dispersion rate when compared to measured data and how the MMPE model is predicting a slightly less dispersion rate than measured data. Furthermore, the BELLHOP/JONSWAP model has a negative intercept with the y-axis, whereas the MMPE has a positive intercept, and the measured data extrapolates to approximately zero.

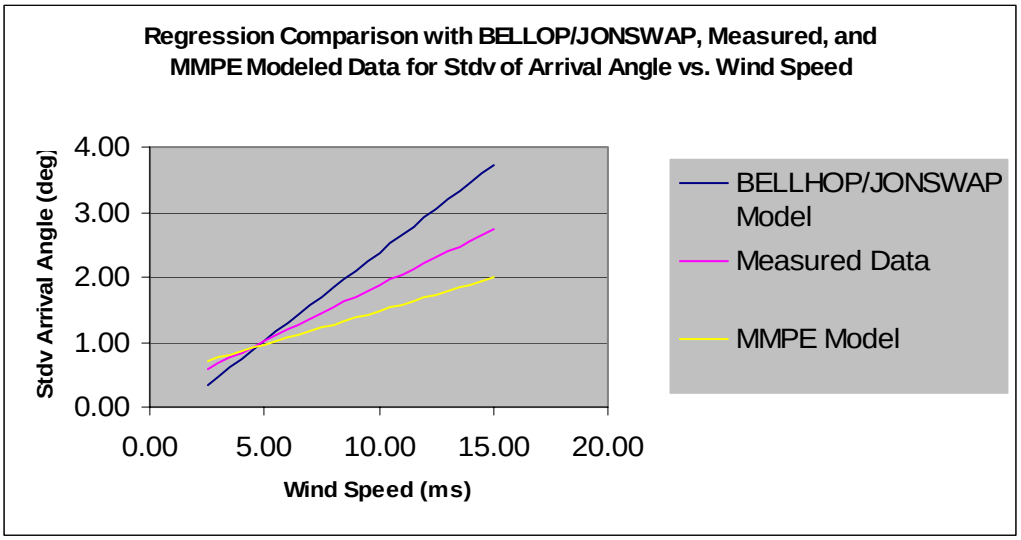

Figure 5.18 Regression Analysis Comparing Standard Deviation of Arrival Angle vs. Wind Speed for BELLHOP/JONSWAP, Measured, and MMPE Modeled Data

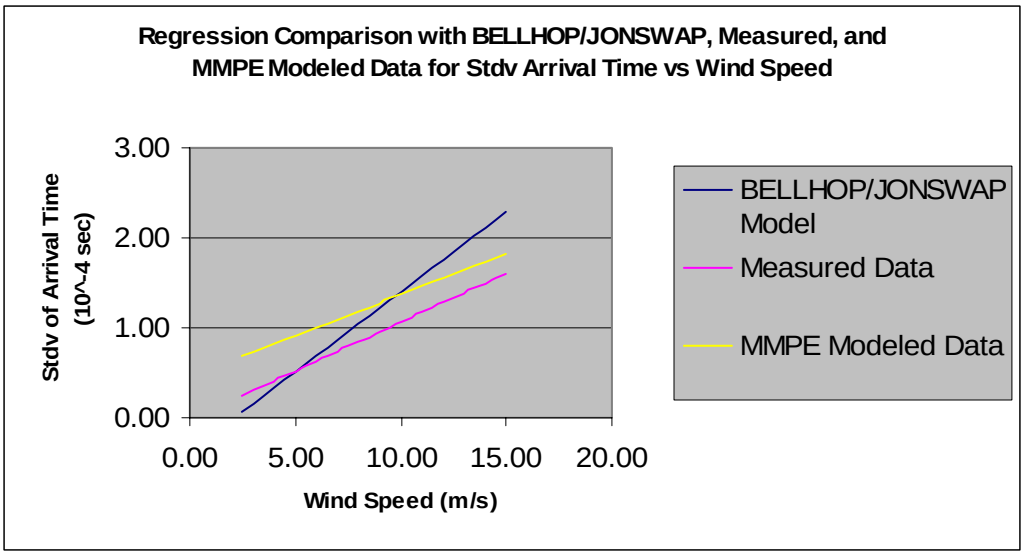

Figure 5.19 Regression Analysis Comparing Standard Deviation of Arrival Time vs. Wind Speed for BELLHOP/JONSWAP, Measured, and MMPE Modeled Data

Although the details of the BELLHOP/JONSWAP model and corresponding data analysis are not available here, we can make several comments on the issues related to the MMPE implementation. It was previously noted that the MMPE surface scatter implementation requires an ad-hoc minimum surface displacement sampling of 1/5. The effect this has on the results is unknown, but may be expected to introduce the most errors at small surface displacements (i.e., small wind speeds). It was also noted that the variability analysis may capture numerical noise which could also affect the low wind speed results. Both of these could contribute to the non-zero variability intercept of the MMPE results.

In spite of these potential issues, the MMPE/JONSWAP model produced results consistent with the measured data and, arguably, as good as the BELLHOP/JONSWAP model predictions. It is also useful to note some comparison between the BELLHOP and MMPE predictions. In both cases, the predicted rate of increase of variability in both arrival angle and arrival time is higher using the BELLHOP model than the MMPE model. This could be due to the higher sensitivity of the ray-based model, although there is no direct evidence of this. Furthermore, the predicted rate of increase of variability in

the arrival time from the MMPE model matched the measured data quite well, while the slope of the BELLHOP results is significantly larger.

VI. CONCLUSIONS AND RECOMMENDATIONS

The littoral waters are challenging acoustically with sea surface motion constantly changing. Developing models that can predict the physical acoustic behavior of this medium with some significant degree of accuracy is a complex effort. The approach taken by this thesis is to build upon existing work related to the Monterey Miami Parabolic Equation model. In each of the chapters in this thesis, analysis has been presented followed by model implementation discussions and results.

Background information about the MMPE was provided as a means to establish a baseline upon which the advanced work of developing sea surface models could be built. A static rough surface forward scatter model was developed which displayed increases in sea surface acoustic scatter as the rms roughness input parameter was increased. A CW test of scattering from a sinusoidal surface was conducted with the results showing reflected rays due to Bragg scatter traveling in distinct directions, as expected. As the surface was allowed to move dynamically, the directions or angles changed but the distinction remained evident. Analysis was conducted on the scattered field from the moving sinusoidal surface and Doppler shifts were determined to be in agreement with calculated Bragg scatter conditions.

In Section V an empirical fetch-limited ocean wave spectrum (JONSWAP) was presented. Model parameters from the HFA97 experiment were used as input and compared with measured data. The results look promising and clearly show dispersion of energy associated with single surface reflected rays as wind speed increases, and clearly show how the direct path (non-surface interaction) remains unchanged. A comparison of linear regression analysis of measured data with MMPE modeled data shows that not only acoustical energy dispersion increases with increasing wind speed, but also how the steepness of the slope of the measured data and modeled data relates to the rate of acoustical energy dispersion. The MMPE/JONSWAP predictions of energy dispersion rates seemed to compare quite favorably for the variability of acoustic travel time. However, the predicted rate for arrival angle variability was too low.

The two MATLAB algorithms that compute arrival angle and arrival time statistics for the MMPE model data are considered good approximations but are not exact. Furthermore, the MMPE results had higher accuracy in arrival time measurements than arrival angle. A combination of these issues, and perhaps others, may be the cause of the underestimate of energy dispersion in predicted arrival angle.

Finally, a regression analysis comparison was made of the BELLHOP/JONSWAP model, the measured data from the HFA97 experiment, and the MMPE model for both the standard deviation of arrival angle and the standard deviation of arrival time vs. wind speed. By examining the slopes of the three curves, the BELLHOP/JONSWAP model predicts a greater dispersion rate than the MMPE model in both cases. Furthermore, the BELLHOP/JONSWAP model was observed to have a negative intercept with the y axis, whereas the MMPE had a positive intercept and the measured data extrapolates to approximately zero. It is unclear why both numerical models missed a physically plausible zero intercept.

The results presented show that surface scatter can significantly affect arrival time, arrival angle, and frequency spread that leads to degradation of acoustic signal coherence. Acoustical communication systems can benefit from models predicting the environmental conditions affecting coherence and potentially these systems can adjust or compensate for the existing conditions.

Some recommendations for future work include examining Doppler shifts for the dynamically evolving rough surface, improving upon the window/slice statistical MATLAB algorithms or examining another approach for determining standard deviation of arrival angle and arrival time, and validating the algorithms with additional measured data.

LIST OF REFERENCES

Badiey, M., Mu, Y., Simmen, J. A., and Forsythe, S.E., "Signal Variability in Shallow-Water Sound Channels," *IEEE Ocean Eng.* **25** (4), pp. 492-500, 2000.

Hardin, R.H. and Tappert, F.D., "Applications of the Split-Step Fourier method to the Numerical Solution of Nonlinear and Variable Coefficient Wave Equations," *SIAM* **Rev. 15**, pp. 423, 1973.

Hasselmann, K., Barnett, T.P., Bouws, E., Carlson, H., Cartwright, D.E., Enke, K., Ewing, J.A., Gienapp, H., Hasselmann, D.E., Kruseman, P., Meerburg, A., Müller, P., Olbers, D.J., Richter, K., Sell, W., and Walden, H., "Measurements of wind-wave growth and swell decay during the Joint North Sea Wave Project (JONSWAP)", *Dtsch. Hydrogr. Z.* **12**, pp. 95, 1973.

Heitsenrether, R., and Badiey, M., "Modeling Acoustic Fluctuations Induced by Sea Surface Roughness", Proceedings of *High Frequency Ocean Acoustics Conference*, March, 2004.

Jensen, F.B., Kuperman W.A., Porter M.B., and Schmidt, H., *Computational Ocean Acoustics*, AIP Press, 2000.

Liebermann, L.N., " Analysis of Rough Surfaces by Scattering," *J. Acoust. Soc. Am.* **35**, pp. 932, 1963.

Marsh, H.W., "Sound Reflection and Scattering from the Sea Surface," *J. Acoust. Soc. Am.* **35**, pp. 240-244, 1963.

Medwin, M., and Clay, C.S., *Fundamentals of Acoustical Oceanography*, Academic Press, pp. 119-124, 1998.

Pierson, W.J., and Moskowitz L., " A Proposed Spectral Form for Fully Developed Wind Seas Based on the Similarity Theory of S. A. Kitaigorodskii, " *J. Geophy. Res.* **69**, pp. 5181-5190, 1964.

Smith, K.B., and Tappert, F.D., "UMPE: The University of Miami Parabolic Equation Model, Version 1.1", *Marine Physical Laboratory Technical Memorandum* **432,** May 1993, rev. Sept. 1993.

Smith, K.B., "Convergence stability , and variability of shallow water acoustic predictions using a split-step Fourier parabolic equation model, " *J. Comp. Acoust.*, Vol. **9**, No. 1, pp. 243-285, 2001.

Tappert, F.D., "Parabolic Approximation Method," in Lecture Notes in Physics, Vol. **70**, *Wave Propagation and Underwater Acoustics,* edited by J.B. Keller and J.S. Papadakis (Springer-Verlag, New York), pp. 224-287, 1977.

Tappert, F.D., and Nghiem-Phu, L., "A new split-step Fourier algorithm for solving the parabolic wave equation with rough surface scattering," *J. Acoust. Soc. Am.* Suppl. **1 77, pp.** S101, 1985.

Thomson, D.J., and Chapman, N.R., "A wide-angle split-step algorithm for the parabolic equation," *J. Acoust. Soc. Am.* **74**(6), pp. 1848-1854, 1983.

Warfield, J.T., " Doppler Shifting of Surface Scattered Reverberation", *U.S. Navy Journal of Underwater Acoustics,* pp. 183-205, 1981.

APPENDIX A. DATA PROCESSING

****

MATLAB Program for Computing Standard Deviation of Arrival Angle

```
%CompAngleSTDVrev6st.m computes the standard deviation of arrival angle in degrees.
%Runs in conjunction with PEOUT2

clear tlpressbeamtst1;
clear tlpressbeamtst2;

for n6=138:1:140;  % Corresponds to window slice of 0.00012 seconds per increment or 0.00036 secs.
   for n5=180:1:240;  % by positive angle of zero to 39.5 degrees
      % Grab slice
      n10=n5-179;
      n11=n6-137;
      tlpressbeamtst2(n10,n11)=tlpressbeam(n5,n6);
   end
end

Amin=min(tlpressbeamtst2); % Find least value of TL
Bmin=min(Amin)

threshold11=Bmin+1;  % thresholds established for 12 bins of 1 db ref to min TL
threshold12=Bmin+2;
threshold13=Bmin+3;
threshold14=Bmin+4;
threshold15=Bmin+5;
threshold16=Bmin+6;
threshold17=Bmin+7;
threshold18=Bmin+8;
threshold19=Bmin+9;
threshold20=Bmin+10;
threshold21=Bmin+11;
threshold22=Bmin+12;


emp=20;  % emphasis value placed on higher TL values; Adds linearity to computation
n7=0;    % at higher windspeeds
```

```
for n6=138:1:140;  % Corresponds to window slice of 0.00036 seconds
for n5=180:1:240;  % by positive angle of zero to 39.5 degrees

   n10=n5-179;
   n11=n6-137;
   tlpressbeamtst1(n10,n11)=tlpressbeam(n5,n6);

   if tlpressbeam(n5,n6)<threshold11;
      n8=n7+32; % weighting of 32 times for transmission loss level below Bmin
+ 1 db
      if n7==0;
         n7=1;
      end
      for n9=n7:1:n8;
         Etest(n9)=theta(n5);
      end
      n7=n8;
   else
      if tlpressbeam(n5,n6)<threshold12;
         n8=n7+25; % weighting of 25 times
         if n7==0;
            n7=1;
         end
         for n9=n7:1:n8;
            Etest(n9)=theta(n5);
         end
         n7=n8;
      else
         if tlpressbeam(n5,n6)<threshold13;
            n8=n7+20;  % weighting of 20
            if n7==0;
               n7=1;
            end
            for n9=n7:1:n8;
            Etest(n9)=theta(n5);
            end
            n7=n8;
         else
            if tlpressbeam(n5,n6)<threshold14;
               n8=n7+16; % weighting of 16
               if n7==0;
                  n7=1;
               end
               for n9=n7:1:n8;
```

```
      Etest(n9)=theta(n5);
   end
   n7=n8;

else
   if tlpressbeam(n5,n6)<threshold15;
      n8=n7+13; % weighting of 13
      if n7==0;
         n7=1;
      end
      for n9=n7:1:n8;
         Etest(n9)=theta(n5);
      end
      n7=n8;
   else
      if tlpressbeam(n5,n6)<threshold16;
         n8=n7+10; % weighting of 10
         if n7==0;
            n7=1;
         end
         for n9=n7:1:n8;
            Etest(n9)=theta(n5);
         end
         n7=n8;
      else
         if tlpressbeam(n5,n6)<threshold17;
            n8=n7+8+emp;  % weighting of 8 plus emphasis value
            if n7==0;
               n7=1;
            end
            for n9=n7:1:n8;
               Etest(n9)=theta(n5);
            end
            n7=n8;

         else
            if tlpressbeam(n5,n6)<threshold18;
               n8=n7+6+emp;  % weighting of six plus emphasis value
               if n7==0;
                  n7=1;
               end
               for n9=n7:1:n8;
                  Etest(n9)=theta(n5);
               end
               n7=n8;
            else
```

```
                    if tlpressbeam(n5,n6)<threshold19;
                       n8=n7+5+emp;  % weighting of 5 plus emphasis value
                       if n7==0;
                          n7=1;
                       end
                       for n9=n7:1:n8;
                          Etest(n9)=theta(n5);
                       end
                       n7=n8;
                    else
                       if tlpressbeam(n5,n6)<threshold20;
                          n8=n7+4+emp; % weighting of 4 plus emphasis value
                          if n7==0;
                             n7=1;
                          end
                          for n9=n7:1:n8;
                             Etest(n9)=theta(n5);
                          end
                          n7=n8;
                       else
                          if tlpressbeam(n5,n6)<threshold21;
                             n8=n7+3+emp;  % weighting of 3 plus emphasis
value
                             if n7==0;
                                n7=1;
                             end
                             for n9=n7:1:n8;
                                Etest(n9)=theta(n5);
                             end
                             n7=n8;
                          else
                             if tlpressbeam(n5,n6)<threshold22;
                                n8=n7+3+emp; % weighting of 3 plus emphasis
value
                                if n7==0;
                                   n7=1;
                                end
                                for n9=n7:1:n8;
                                   Etest(n9)=theta(n5);
                                end
                                n7=n8;
                             end
                          end

                       end
```

```
                    end

                  end
                end
              end

            end

          end

        end
      end
    end
  end
end
```

```
Angtest=std(Etest)% compute standard deviation of arrival angle
clear Etest
**********************************************************************
```

MATLAB Program for Computing Standard Deviation of Time of Arrival

```
 %CompTimeSTDV computes the standard deviation of time of arrival and runs
% in conjunction with PEOUT2

clear tlpressbeamtst1;
clear tlpressbeamtst2;

for n6=138:1:140;  % Corresponds to window slice of 0.00012 seconds per
increment
            % or 0.00036 secs.
  for n5=180:1:240;  % by positive angle of zero to 39.5 degrees

    n10=n5-179;
    n11=n6-137;
    tlpressbeamtst2(n10,n11)=tlpressbeam(n5,n6);
  end
end

Amin=min(tlpressbeamtst2); % Find least value of TL
Bmin=min(Amin)

threshold11=Bmin+1;  % thresholds established for 12 bins of 1 db ref to min TL
threshold12=Bmin+2;
```

```
threshold13=Bmin+3;
threshold14=Bmin+4;
threshold15=Bmin+5;
threshold16=Bmin+6;
threshold17=Bmin+7;
threshold18=Bmin+8;
threshold19=Bmin+9;
threshold20=Bmin+10;
threshold21=Bmin+11;
threshold22=Bmin+12;


emp=0    % emphasis value, zero means no emphasis added
n7=0;




for n6=138:1:140;  % Corresponds to window slice of 0.00036 seconds
for n5=180:1:240;  % by positive angle of zero to 39.5 degrees

   n10=n5-179;
   n11=n6-137;
   tlpressbeamtst1(n10,n11)=tlpressbeam(n5,n6);

   if tlpressbeam(n5,n6)<threshold11;
      n8=n7+32; % weighting of 32 times for transmission loss level below Bmin
+ 1 db
      if n7==0;
         n7=1;
      end
      for n9=n7:1:n8;
         Ftest(n9)=timeout(n5);
      end
      n7=n8;
   else
      if tlpressbeam(n5,n6)<threshold12;
         n8=n7+25; % weighting of 25 times
         if n7==0;
            n7=1;
         end
         for n9=n7:1:n8;
             Ftest(n9)=timeout(n5);
         end
         n7=n8;
      else
```

```
if tlpressbeam(n5,n6)<threshold13;
   n8=n7+20;  % weighting of 20 times
   if n7==0;
      n7=1;
   end
   for n9=n7:1:n8;
    Ftest(n9)=timeout(n5);
   end
   n7=n8;
else
   if tlpressbeam(n5,n6)<threshold14;
      n8=n7+16; % weighting of 16 times
      if n7==0;
         n7=1;
      end
      for n9=n7:1:n8;
          Ftest(n9)=timeout(n5);
      end
      n7=n8;

   else
      if tlpressbeam(n5,n6)<threshold15;
         n8=n7+13; % weighting of 13 times
         if n7==0;
            n7=1;
         end
         for n9=n7:1:n8;
             Ftest(n9)=timeout(n5);
         end
         n7=n8;
      else
         if tlpressbeam(n5,n6)<threshold16;
            n8=n7+10; % weighting of 10 times
            if n7==0;
               n7=1;
            end
            for n9=n7:1:n8;
                Ftest(n9)=timeout(n5);
            end
            n7=n8;
         else
            if tlpressbeam(n5,n6)<threshold17;
               n8=n7+8+emp; % weighting of 8 times
               if n7==0;
                  n7=1;
               end
```

```
    for n9=n7:1:n8;
        Ftest(n9)=timeout(n5);
    end
    n7=n8;

else
    if tlpressbeam(n5,n6)<threshold18;
        n8=n7+6+emp;  % weighting of 6 times
        if n7==0;
            n7=1;
        end
        for n9=n7:1:n8;
            Ftest(n9)=timeout(n5);
        end
        n7=n8;
    else
        if tlpressbeam(n5,n6)<threshold19;
            n8=n7+5+emp;  % weighting of 5 times
            if n7==0;
                n7=1;
            end
            for n9=n7:1:n8;
                Ftest(n9)=timeout(n5);
            end
            n7=n8;
        else
            if tlpressbeam(n5,n6)<threshold20;
                n8=n7+4+emp;  % weighting of 4 times
                if n7==0;
                    n7=1;
                end
                for n9=n7:1:n8;
                    Ftest(n9)=timeout(n5);
                end
                n7=n8;
            else
                if tlpressbeam(n5,n6)<threshold21;
                    n8=n7+3+emp;  % weighting of 3 times
                    if n7==0;
                        n7=1;
                    end
                    for n9=n7:1:n8;
                        Ftest(n9)=timeout(n5);
                    end
                    n7=n8;
                else
```

```
                        if tlpressbeam(n5,n6)<threshold22;
                           n8=n7+3+emp;  % weighting of 3 times
                           if n7==0;
                              n7=1;
                           end
                           for n9=n7:1:n8;
                               Ftest(n9)=timeout(n5);
                           end
                           n7=n8;
                        end
                     end

                  end

               end

            end
         end
      end

   end

  end
 end
end
end


Timtest=std(Ftest)% compute standard deviation of arrival time
clear Ftest
```

THIS PAGE INTENTIONALLY LEFT BLANK

APPENDIX B. LINEAR REGRESSION STATISICAL ANALYSIS

****

Standard Deviation of Arrival Angle vs. Wind Speed for MMPE Model Data

SUMMARY OUTPUT

Regression Statistics	
Multiple R	0.986387
R Square	0.972959
Adjusted R Square	0.968452
Standard Error	0.093242
Observations	8

ANOVA

	df	*SS*	*MS*	*F*	*Significance F*
Regression	1	1.876923	1.876923	215.8833	6.24E-06
Residual	6	0.052165	0.008694		
Total	7	1.929088			

	Coefficients	*Standard Error*	*t Stat*	*P-value*	*Lower 95%*	*Upper 95%*
Intercept	0.450394	0.066487	6.77415	0.000506	0.287706	0.613083
X Variable 1	0.102831	0.006999	14.69297	6.24E-06	0.085706	0.119956

RESIDUAL OUTPUT

Observation	*Predicted Y*	*Residuals*
1	0.553225	0.006775
2	0.758887	-0.00889
3	0.964549	0.035451
4	1.170211	-0.13021
5	1.478704	0.091296
6	1.684366	0.005634
7	1.787197	0.112803
8	1.992859	-0.11286

****

Standard Deviation of Arrival Time vs. Wind Speed for MMPE Model Data

SUMMARY OUTPUT

Regression Statistics	
Multiple R	0.977426
R Square	0.955361
Adjusted R Square	0.947921
Standard Error	0.106244
Observations	8

ANOVA

	df	*SS*	*MS*	*F*	*Significance F*
Regression	1	1.449474	1.449474	128.4118	2.83E-05
Residual	6	0.067726	0.011288		
Total	7	1.5172			

	Coefficients	*Standard Error*	*t Stat*	*P-value*	*Lower 95%*	*Upper 95%*
Intercept	0.464479	0.075758	6.131106	0.000861	0.279106	0.649852
X Variable 1	0.090366	0.007975	11.33189	2.83E-05	0.070853	0.109879

RESIDUAL OUTPUT

Observation	*Predicted Y*	*Residuals*
1	0.554845	-0.02485
2	0.735577	-0.09558
3	0.91631	0.10369
4	1.097042	-0.05704
5	1.368141	0.161859
6	1.548873	0.021127
7	1.639239	0.020761
8	1.819972	-0.12997

****

Standard Deviation of Arrival Angle vs. Wind Speed for Measured HFA97 Data

SUMMARY OUTPUT

Regression Statistics	
Multiple R	0.832309
R Square	0.692738
Adjusted R Square	0.679378
Standard Error	0.439401
Observations	25

ANOVA

	df	*SS*	*MS*	*F*	*Significance F*
Regression	1	10.01175	10.01175	51.85459	2.48E-07
Residual	23	4.44069	0.193073		
Total	24	14.45244			

	Coefficients	*Standard Error*	*t Stat*	*P-value*	*Lower 95%*	*Upper 95%*
Intercept	0.155232	0.21186	0.732711	0.471137	-0.28303	0.593498
X Variable 1	0.171888	0.02387	7.201013	2.48E-07	0.122509	0.221267

RESIDUAL OUTPUT

Observation	*Predicted Y*	*Residuals*
1	0.385562	-0.38556
2	0.385562	-0.18556
3	0.316807	-0.11681
4	1.038737	-0.09874
5	0.923572	-0.09357
6	0.923572	0.206428
7	0.923572	0.386428
8	1.153902	0.346098
9	1.315476	0.184524
10	1.461581	0.413419
11	1.499397	-0.5594
12	1.499397	-0.3694
13	1.691911	-0.19191
14	1.769261	0.480739
15	1.844892	0.235108
16	1.844892	-0.71489
17	1.922241	0.327759
18	1.922241	0.707759
19	2.07694	-0.19694

20	2.152571	0.097429
21	2.152571	0.097429
22	2.152571	0.657429
23	2.30727	-0.05727
24	2.460251	-1.15025
25	2.460251	-0.02025

****

Standard Deviation of Arrival Time vs. Wind Speed for Measured HFA97 Data

SUMMARY OUTPUT

Regression Statistics	
Multiple R	0.877373
R Square	0.769784
Adjusted R Square	0.757668
Standard Error	0.217574
Observations	21

ANOVA

	df	*SS*	*MS*	*F*	*Significance F*
Regression	1	3.007481	3.007481	63.53124	1.77E-07
Residual	19	0.899434	0.047339		
Total	20	3.906914			

	Coefficients	*Standard Error*	*t Stat*	*P-value*	*Lower 95%*	*Upper 95%*
Intercept	-0.02323	0.114162	-0.20351	0.840896	-0.26218	0.21571
X Variable 1	0.108426	0.013603	7.970649	1.77E-07	0.079954	0.136898

RESIDUAL OUTPUT

Observation	*Predicted Y*	*Residuals*
1	0.098204	0.181796
2	0.145911	0.134089
3	0.170849	-0.17085
4	0.461432	-0.27143
5	0.461432	-0.18143
6	0.485285	0.174715
7	0.606723	-0.13672
8	0.704306	-0.14431

9	0.800806	-0.05081
10	0.800806	-0.05081
11	0.849598	0.090402
12	0.946097	-0.0061
13	0.994889	0.225111
14	1.018742	-0.17874
15	1.067534	-0.03753
16	1.067534	0.242466
17	1.04303	0.64697
18	1.188972	-0.05897
19	1.212825	-0.08283
20	1.334263	-0.11426
21	1.430762	-0.21076

****

Standard Deviation of Arrival Angle vs. Wind Speed for BELLHOP/JONSWAP Model Data

Multiple R	0.983743
R Square	0.96775
Adjusted R Square	0.965269
Standard Error	0.169868
Observations	15

ANOVA

	df	*SS*	*MS*	*F*	*Significance F*
Regression	1	11.25626	11.25626	390.0964	4.45E-11
Residual	13	0.375116	0.028855		
Total	14	11.63137			

	Coefficients	*Standard Error*	*t Stat*	*P-value*	*Lower 95%*	*Upper 95%*
Intercept	-0.33638	0.127809	-2.63193	0.020711	-0.6125	-0.06027
X Variable 1	0.271122	0.013727	19.75086	4.45E-11	0.241466	0.300778

RESIDUAL OUTPUT

Observation	*Predicted Y*	*Residuals*
1	0.476981	-0.19698

2	0.699301	-0.1393
3	1.14123	-0.02123
4	1.439464	-0.03946
5	1.58587	0.19413
6	1.808189	0.001811
7	1.881392	0.068608
8	2.030509	0.059491
9	2.103712	0.126288
10	2.326032	0.043968
11	2.472438	0.037562
12	2.767961	0.162039
13	2.917078	0.152922
14	3.212601	-0.0026
15	3.657241	-0.44724

****

Standard Deviation of Arrival Time vs. Wind Speed for BELLHOP/JONSWAP Model Data

Standard Error	0.16319
Observations	18

ANOVA

	df	*SS*	*MS*	*F*	*Significance F*
Regression	1	7.706266	7.706266	289.3727	1.14E-11
Residual	16	0.426095	0.026631		
Total	17	8.132361			

	Coefficients	*Standard Error*	*t Stat*	*P-value*	*Lower 95%*	*Upper 95%*
Intercept	-0.39017	0.100389	-3.88659	0.00131	-0.60299	-0.17736
X Variable 1	0.179012	0.010523	17.01096	1.14E-11	0.156704	0.20132

RESIDUAL OUTPUT

Observation	*Predicted Y*	*Residuals*
1	0.205938	-0.11594
2	0.256062	-0.06606
3	0.306185	-0.11618
4	0.404641	-0.03464

5	0.605135	-0.04513
6	0.703592	0.036408
7	0.902295	0.117705
8	1.002542	0.117458
9	1.201245	0.008755
10	1.299701	0.000299
11	1.399948	0.090052
12	1.500195	-0.01019
13	1.598651	0.071349
14	1.698898	0.341102
15	1.897601	0.142399
16	1.996058	0.043942
17	2.096305	-0.1463
18	2.295008	-0.43501

THIS PAGE INTENTIONALLY LEFT BLANK

INITIAL DISTRIBUTION LIST

1. Defense Technical Information Center
   Ft. Belvoir, VA

2. Dudley Knox Library
   Naval Postgraduate School
   Monterey, CA

3. Dr. Kevin B. Smith
   Naval Postgraduate School
   Monterey, CA

4. Dr. Daniel T. Nagle
   Naval Undersea Warfare Center Division Newport
   Newport, RI

5. Dr. Mohsen Badiey
   University of Delaware
   Newark, DE

6. Dr. Ellen Livingston
   Office of Naval Research
   Arlington, VA

7. Technical Library
   Naval Undersea Warfare Center Division Newport
   Newport, RI